



1 Secondary organic aerosol production from pinanediol, a semi-

2 volatile surrogate for first-generation oxidation products of

3 monoterpenes

4 Penglin Ye^a, Yunliang Zhao, Wayne K. Chuang, Allen L. Robinson, Neil M. Donahue*

5 Center for Atmospheric Particle Studies, Carnegie Mellon University, 5000 Forbes Avenue, Pittsburgh,
6 Pennsylvania 15213, United States

^anow at: Aerodyne Research Inc, Billerica, MA 01821, USA

8

9

10

11

12

13

14

15

16

17

*Correspondence to: nmd@andrew.cmu.edu

17



18 **Abstract**

19 We have investigated the production of secondary organic aerosol (SOA) from pinanediol
20 (PD), a precursor chosen as a semi-volatile surrogate for first-generation oxidation
21 products of monoterpenes. Observations at the CLOUD facility at CERN have shown that
22 oxidation of organic compounds such as PD can be an important contributor to new-particle
23 formation. Here we focus on SOA mass yields and chemical composition from PD photo-
24 oxidation in the CMU smog chamber. To determine the SOA mass yields from this semi-
25 volatile precursor, we had to address partitioning of both the PD and its oxidation products
26 to the chamber walls. After correcting for these losses, we found OA loading dependent
27 SOA mass yields from PD oxidation that ranged between 0.1 and 0.9 for SOA
28 concentrations between 0.02 and 20 $\mu\text{g m}^{-3}$, these mass yields are 2–3 times larger than
29 typical of much more volatile monoterpenes. The average carbon oxidation state measured
30 with an Aerosol Mass Spectrometer was around -0.7. We modeled the chamber data using
31 a dynamical two-dimensional volatility basis set and found that a significant fraction of the
32 SOA comprises low volatility organic compounds that could drive new-particle formation
33 and growth, which is consistent with the CLOUD observations.



34 1 Introduction

35 Particulate matter (PM) in the atmosphere affects human health and life expectancy (Pope
36 et al., 2009) and also influences Earth's climate by absorbing and scattering radiation
37 (Solomon, 2007). Organic compounds constitute a large fraction of that PM, making up
38 around 20–90% of the aerosol mass in the lower troposphere (Kanakidou et al., 2005).

39 Secondary organic aerosol (SOA), formed from oxidation of gas-phase organic compounds
40 in the atmosphere, accounts for a significant fraction of the organic aerosol (OA) in PM
41 (Zhang et al., 2007). In the atmosphere, OA is dynamic due to constant photo-oxidation
42 and associated evolution in thermodynamic properties (Seinfeld and Pandis, 2006;
43 Donahue et al., 2005). However, classical smog-chamber experiments encompass only the
44 early stages of SOA formation, including one generation or at most a few generations of
45 oxidation chemistry (Pandis et al., 1991; Odum et al., 1996a). While those experiments
46 may include some later-generation chemistry, the commonly used two-product model
47 (Odum et al., 1996a) treats the (quasi) first-generation products as effectively non-reactive.

48 Further oxidation (aging) of SOA may add more functional groups to the carbon backbone,
49 causing the second-generation oxidation products to be even less volatile and more water
50 soluble than the first-generation products, which will also enhance the SOA mass (Donahue
51 et al., 2005). However, ongoing oxidation must eventually fragment products and drive
52 down the SOA mass because the end state of organic oxidation is CO₂ formation (Kroll et
53 al., 2009; Chacon-Madrid et al., 2012; Donahue et al., 2013). There is considerable
54 evidence that the ongoing oxidation chemistry can increase SOA mass and oxidation state,
55 both from smog-chamber experiments (Donahue et al., 2012a; Henry and Donahue, 2012;
56 Qi et al., 2012) and also from flow tubes that simulate many days of oxidation using intense



57 UV radiation to drive photochemistry (Lambe et al., 2011; Wong et al., 2011; Cubison et
58 al., 2011). The flow-tube results also confirm that oxidation will eventually cause mass
59 loss via fragmentation (Tkacik et al., 2014). The volatility basis set (VBS) was developed
60 to treat this ongoing chemistry by condensing the enormous ensemble of organic
61 compounds involved onto a basis grid described by volatility and the carbon oxidation state
62 (Donahue et al., 2006; Donahue et al., 2011a; Donahue et al., 2012b; Chuang and Donahue,
63 2016b; Tröstl et al., 2016), with coupling constants constrained by chemical behavior of
64 representative or average compounds (Chacon-Madrid et al., 2012; Donahue et al., 2013).

65 Bulk SOA aging experiments show that later-generation chemistry will influence SOA
66 properties, but those experiments provide limited mechanistic insight due to the extreme
67 complexity of the chemistry involving multiple generations of multiple products. A
68 complementary approach is to use selected first-generation products from SOA formation
69 to probe second-generation chemistry systematically, and to proceed through
70 representative later-generation products. For example, the known products of α -pinene
71 oxidation include pinonaldehyde, which is one of the most volatile products, and acids such
72 as cis-pinonic acid and pinic acid which are some of the least volatile monomer products
73 (Jang and Kamens, 1999; Jaoui and Kamens, 2001). Smog-chamber experiments at
74 Carnegie Mellon have shown that pinonaldehyde is a modest but significant source of SOA
75 at both high NO (Chacon-Madrid and Donahue, 2011) and low NO (Chacon-Madrid et al.,
76 2013) conditions. Aldehyde chemistry is dominated by OH radical attack on the terminal -
77 CHO moiety, causing fragmentation (Chacon-Madrid et al., 2010), but OH attack along
78 the carbon backbone leads to functionalized products that condense to enhance SOA
79 formation from the first-generation parent α -pinene, with mass yields of roughly 10%



under atmospherically relevant conditions. If the most volatile α -pinene product can enhance SOA production, it stands to reason that less volatile SVOC products would have an even greater effect. Indeed, we have observed very low volatility products from cis-pinonic acid oxidation, such as MBTCA (Müller et al., 2012), but we have not systematically explored the SOA mass yields from first-generation SVOC products. Here we use pinanediol (PD) as a surrogate for semi-volatile first-generation oxidation products of monoterpenes to study this aging chemistry. PD has a volatility similar to cis-pinonic acid ($C^* \sim 300 \mu\text{g m}^{-3}$) but it is commercially available and easier to handle.

One reason that SOA mass yields from SVOCs are not commonly reported is that SVOCs are hard to handle and measure, and mass-yield determinations require accurate values for the amount of oxidized precursor because the mass yield by definition is the ratio of formed SOA to oxidized precursor mass. There are two reasons why this is challenging for SVOCs. First, they are sticky and hard to measure. Second, and more challenging, SVOCs may be lost to Teflon chamber walls (Matsunaga and Ziemann ‡, 2010) and may even return from the chamber walls as oxidation perturbs a putative gas-Teflon equilibrium. This means any measured change in the SVOC concentration, even if an instrument is well characterized, may not reflect the actual amount of oxidized SVOC.

Sorption of SVOCs into Teflon chamber walls has recently become a matter of significant concern. Matsunaga and Ziemann (2010) showed that various organic compounds broadly in the intermediate volatility range (IVOCs, (Donahue et al., 2011a)) appear to sorb reversibly to Teflon chamber walls, and more recent work has confirmed this finding. The fraction of organic vapors left in gas phase appears to depend on the volatility and the molecular structure of the organics, but Matsunaga and Ziemann suggested that IVOCs



partition into a disrupted surface layer of the Teflon as if the Teflon had an equivalent mass of between 2 and 10 mg m⁻³, depending on molecular structure (for a several cubic meters chamber). As an example, an 8 m³ chamber has a surface area of 12 m², and if the disrupted Teflon surface layer postulated by Matsunaga and Ziemann were 1 µm thick it would have a volume of 12 x 10⁻⁶ m³ and thus a mass of roughly 10 g; projected to the chamber volume this gives an equivalent mass concentration of roughly 1 g m⁻³. To have an effective "partitioning mass" of 1-10 mg m⁻³ this material would thus need to have a mass-based activity coefficient of 100-1000 (Trump et al., 2016). This is consistent with weak interactions involving non-polarizable Teflon and also a low degree of interactions among sorbed organics within the walls at the Henry's law, low-concentration limit. However, we must stress that the exact mechanism of organic sorption to Teflon chamber walls remains unclear.

More recently, Ye et al. (Ye et al., 2016a) and Krechmer et al. (Krechmer et al., 2016) showed that SVOCs are lost to the Teflon walls steadily, with a time constant of roughly 15 minutes (again for a several cubic-meter chamber). The SVOCs in these studies had 1 < C* < 300 µg m⁻³ and so would be expected to leave only a small fraction ($\ll 10\%$) in the gas phase; this quasi-irreversible loss is thus broadly consistent with the reversible equilibration reported earlier for IVOCs.

We expect PD to partition substantially to the walls of a Teflon chamber. Even 2-decanol showed significant vapor loss (Matsunaga and Ziemann, 2010), and the additional OH group in PD decreases the vapor saturation concentration of PD by around 2.3 decades (Donahue et al., 2011a). This should cause larger mass loss to the chamber walls. In order to get an accurate SOA mass yield from oxidation of PD, we need to determine how much



126 PD exists in the gas phase vs the chamber walls, and ultimately how much PD reacts during
127 SOA formation experiments.

128 Another reason we are interested in SOA formation from PD is that it has already been
129 used as a surrogate for the first-generation terpene oxidation products to explore the role
130 of gas-phase aging in new-particle formation, and we wish to compare SOA formation with
131 new-particle formation. The Cosmics Leaving OUtdoor Droplets (CLOUD) facility at
132 CERN is designed to study the effects of cosmic rays on new-particle formation (nucleation
133 and growth) (Kirkby et al., 2011; Duplissy et al., 2016). Early experiments focused on
134 sulfuric acid vapor and different stabilizing species that include the ammonia, amines and
135 oxidation products of organic precursors (Kirkby et al., 2011; Schobesberger et al., 2013;
136 Riccobono et al., 2014). PD was used to mimic first-generation oxidation products of
137 monoterpenes formed in the atmosphere (Schobesberger et al., 2013). Specifically the
138 experiments addressed the hypothesis that oxidation of these first-generation products by
139 OH radicals could produce later-generation products with sufficient supersaturation to
140 participate in nucleation (Donahue et al., 2011c). The PD oxidation experiments were
141 among the first to observe highly oxidized, extremely low volatility organic compounds
142 (ELVOCs) (Donahue et al., 2011a), with the original 10 carbon atoms decorated by up to
143 12 oxygen atoms (Schobesberger et al., 2013; Riccobono et al., 2014). The composition of
144 these highly oxidized organic molecules (HOMs) and possible mechanisms for their
145 formation remains an active research topic (Ehn et al., 2014).

146 In this study, we focus on SOA formation following oxidation of PD by OH radicals. Our
147 first objective is to extend our understanding of SOA aging via experiments addressing
148 carefully selected first-generation products from common SOA precursors. Our second



149 objective is to compare the properties of bulk SOA produced at relatively high
150 concentrations ($0.3\text{--}30 \mu\text{g m}^{-3}$) with the PD oxidation products observed condensing onto
151 particles during the CLOUD nucleation experiment. Our third objective is to use PD as a
152 model compound to explore the complications of precursor losses to Teflon walls in smog-
153 chamber SOA formation experiments. We explore the wall sorption of PD by comparing
154 the total amount of PD injected into the chamber to the PD concentration observed in the
155 gas phase. We also investigate the release of sorbed PD from the chamber walls by heating
156 or diluting the chamber. We then calculate the SOA mass yields, accounting for the loss of
157 PD and also the loss of oxidation products to the Teflon chamber walls. Finally, we
158 describe the elemental composition of the formed SOA. We analyze the SOA volatility
159 distribution and oxidation state within the two-dimensional volatility-oxidation set (2D-
160 VBS) and compare the properties of bulk SOA to the ELVOCs observed in CLOUD.

161 **2 Materials and methods**

162 We conducted experiments in the Carnegie Mellon University (CMU) Smog Chamber, a
163 10 m^3 Teflon bag suspended in a temperature-controlled room. The chamber and our
164 methodology have been described extensively in the literature (Hildebrandt et al., 2009).
165 Before each experiment, we cleaned the bag by flushing it with clean, dry air and exposing
166 it to UV irradiation at $\sim 35^\circ\text{C}$. We subsequently maintained the chamber at a constant
167 temperature unless otherwise noted.

168 For the experiments in this paper, we introduced organic compounds into the chamber via
169 a flash vaporizer (Robinson et al., 2013). We used a small, resistive metal heater enclosed
170 in a stainless-steel sheath to evaporate the organics inside the chamber, placing the organics



171 into an indentation on the stainless-steel surface before inserting the heater into the
172 chamber on the end of a long stainless-steel tube. With a flow of clean, dry dispersion air
173 flowing through the tube for mixing, we power-cycled the heater until the organics
174 completely evaporated. For various experiments, we used *n*-tridecane, 1-tridecene, 2-
175 nonanone, 2-nonal, oxy pinocamphone, and pinanediol (Sigma-Aldrich, 99%). For SOA
176 formation experiments we used ammonium sulfate seed particles ((NH₄)₂SO₄, Sigma
177 Aldrich, 99.99%), which we formed by atomizing a 1 g L⁻¹ (NH₄)₂SO₄ solution in ultrapure
178 deionized water to produce droplets that passed through a diffusion dryer and a neutralizer
179 before they entered the chamber. These seed particles served as a condensation sink for
180 condensable vapors in order to reduce vapor wall losses. To form OH radicals during
181 oxidation experiments we added nitrous acid (HONO) to the chamber by bubbling filtered
182 air through a HONO solution for 20 minutes.

183 We measured gas-phase organic species using both a proton-transfer-reaction mass
184 spectrometer (PTRMS, Ionicon Analytik) and a gas chromatograph/mass spectrometer
185 (GC/MS) (Agilent, 6890 GC/5975 MS) equipped with a thermal desorption and injection
186 system (TDGC/MS, Gerstel, MA) and a capillary column (Agilent HP-5MS, 30 m × 0.25
187 mm) (Zhao et al., 2014). We maintained the temperature of the PTRMS inlet line at 60 °C
188 to minimize line losses. For the thermal desorption GC measurements, we collected
189 samples by drawing chamber air through Tenax® TA filled glass tubes (Gerstel 6mm OD,
190 4.5mm ID glass tube filled with ~290 mg of Tenax TA) at a flow rate of 0.5 L min⁻¹ for 2
191 minutes. We tracked the recovery of organics during analysis using C12, C16, C20, C24,
192 C30, C32, C36 deuterated n-alkanes as standards that we spiked into each Tenax tube prior
193 to the thermal desorption.



194 We measured particle number and volume concentrations inside the chamber using a
195 scanning mobility particle sizer (SMPS, TSI classifier model 3080, CPC model 3772 or
196 3010). We measured size-resolved and bulk particle composition and mass concentrations
197 with a high-resolution time-of-flight aerosol mass spectrometer (HR-ToF-AMS, Aerodyne
198 Research, Inc.). We operated the HR-ToF-AMS following the common protocol with the
199 vaporizer temperature at 600 °C and electron ionization at 70 eV. We collected mass
200 spectra and particle time-of-flight (pToF) measurements in V-mode, which provides high
201 mass resolution (2000 m/Δm) and excellent transmission efficiency. We analyzed the AMS
202 data using the SQUIRREL V1.53G and PIKA 1.12G.

203 **3 Results and Discussion**

204 **3.1 Correction for the loss of the precursors, pinanediol, to the Teflon chamber walls.**

205 Because SVOCs should sorb to the Teflon walls, we expect a portion of PD to be lost after
206 PD was injected into our chamber. To constrain this, we injected equal quantities of six
207 compounds into our chamber simultaneously: PD, oxy pinocamphone, *n*-tridecane, 1-
208 tridecene, 2-nonenone, and 2-nonalol. The first two are an SVOC and an IVOC, while the
209 last four are VOCs that should have very limited wall partitioning at equilibrium. We then
210 measured the resulting gas-phase concentrations in the chamber using both TD-GC/MS
211 and PTRMS and compared the observed signals to those we expected based on the injected
212 amounts.

213 In Fig 1. we compare the TD-GC/MS measurements with the amounts of organics we
214 injected. The VOCs, *n*-tridecane, 1-tridecene, 2-nonenone and 2-nonalol, all fall along the
215 1:1 line, demonstrating that they have minimal wall losses and excellent recovery,



216 consistent with our expectations. However, PD and oxy pinocamphone show large
217 discrepancies between the measured and injected amounts. The recovered gas-phase values
218 show that 43% of the injected oxy pinocamphone and 86% of the PD were lost; only 14%
219 of the PD remained in the gas phase.

220 In Fig 2. we show the results of an experiment where we injected a succession of aliquots
221 of 1-tridecene, 2-nonenone, oxy pinocamphone and PD into the chamber, with expected
222 stepwise incremental increases of 11 ppbv each, and measured the gas-phase
223 concentrations with a PTRMS. We observed that the PTRMS signal stabilized after each
224 injection, and each injection with the same amount of organics resulted in a similar step-
225 wise vapor concentration increase. The two VOCs, 1-tridecene and 2-nonenone, both
226 showed concentration increases consistent with expectations. The PTRMS sensitivity to
227 nonenone is higher than its sensitivity to 1-tridecene, and so the signal to noise is
228 substantially higher. The 2-nonenone shows nearly square-wave response with a brief (~ 1
229 min) overshoot related to the chamber mixing timescale, and the 1-tridecene signal
230 displayed the same behavior. Oxy pinocamphone and PD show lower than expected
231 stepwise increases in concentration with a longer rise time. The step-wise increases for oxy
232 pinocamphone and PD are consistent with near constant wall-loss factors in the
233 concentration range in this study, but the signals are not consistent with instantaneous
234 evaporation and subsequent wall partitioning. If that was the case we would expect a large
235 initial spike similar and equal in magnitude to the spike in 2-nonenone (i.e. we would
236 expect the full 11 ppb to appear initially in the gas phase); we would then expect the SVOC
237 signal to drop to an equilibrium value on the equilibrium timescale for wall interactions –
238 10-15 minutes for our chamber (Ye et al., 2016a), as observed by Krechmer et al using a



239 core-flow inlet CIMS and nitrate chemical ionization (Krechmer et al., 2016). The slow
240 increase in signal we observe may be the convolution of two effects: less than instantaneous
241 evaporation from the flash vaporizer for the SVOCs and slow equilibration of the PTRMS
242 sampling line. Regardless, the signals in the PTRMS stabilize to values consistent with the
243 TD-GC/MS results; these experiments are both consistent with relatively rapid, reversible
244 equilibration of SVOCs (represented by the PD) and IVOCs (represented by the oxy
245 pinocamphone) between the gases and the Teflon chamber walls.

246 In order to calculate SOA mass yields, we must determine the amount of precursor oxidized
247 based on the change in precursor signals (e.g. the gas-phase PTRMS measurements). This
248 is straightforward for a VOC with minimal wall interactions, but for the SVOCs we must
249 account for their significant interaction with the Teflon walls. It is not sufficient to simply
250 measure the change in the gas-phase PD concentration, because of the apparently rapid
251 equilibration suggested by the theory put forward by Matsunaga and Ziemann and
252 supported by our wall-loss experiments. If PD were in equilibrium with the walls there
253 would be a substantial source of PD to the gas phase from the Teflon walls as PD was lost
254 from the gas phase due to oxidation or any other sink. Simply put, the results suggest
255 that, at equilibrium, for every 10 units of PD in the gas phase, roughly 100 units are sorbed
256 in or on the Teflon walls. Therefore, removal of a small amount from the gas phase (say 1
257 unit) should result in replenishment of 90% by the walls to maintain the equilibrium.
258 Consequently, if we observe a decrease of 1 unit of PD vapor, that implies that 10 units are
259 actually lost from the gas phase since the evaporation of PD from the Teflon walls re-
260 establish the equilibrium. This, obviously, has large implications for the calculated SOA
261 mass yields above and beyond any possible wall losses for products of the PD oxidation.



262 We use two methods, heating and isothermal dilution, to test whether the Teflon chamber
263 walls in fact serve as an accessible reservoir of PD. Increasing the chamber temperature
264 raises the saturation concentration of PD and thus decreases the activity of PD vapors.
265 Heating by 30 °C should raise the saturation concentration of PD by a factor of 10 to 30
266 and lower the gas-phase activity (the concentration divided by the saturation concentration)
267 by the same factor. Some PD sorbed to the Teflon should then evaporate to lower the
268 condensed-phase activity. To test this, we injected 866 µg m⁻³ (118 ppbv) of PD vapor into
269 the chamber at 13 °C and subsequently increased the chamber temperature to 44 °C. As
270 shown in Fig. 3, the PD vapor concentration measured by the PTRMS increased rapidly
271 after heating and reached a steady value after the temperature stabilized at 44 °C. The
272 concentration rose by a factor of 2.5-3. To be certain that desorption from the walls was
273 the only possible source, we also monitored the suspended aerosol mass using an HR-AMS.
274 The total organic mass in particles was around 5 µg m⁻³, far less than the increase of the
275 PD vapor concentration. Particle evaporation thus contributed negligibly to the increase of
276 PD vapors; therefore, the PD adsorbed or absorbed by the Teflon chamber walls was the
277 only possible source of the increased gas-phase burden.
278 Increasing temperature by 30 °C should increase the saturation concentration (C^*) of PD
279 by roughly a factor of 30 (May et al., 2012). All else being equal, this should cause a 30-
280 fold increase in the activity ratio of the sorbed PD to the gas-phase PD and thus drive a
281 large return flux to the gas phase, with the equilibrium vapor fraction increasing from 13%
282 to around 80%. This is consistent with our observations though we observe a factor of 2-3
283 less than this simple calculation would suggest. However, if PD is absorbed in the Teflon
284 walls, it is likely that the activity coefficient of the PD in Teflon walls would drop



285 substantially upon heating, so this would allow the activities to equilibrate with a smaller
286 net change in absolute concentration. Acknowledging these large uncertainties, the heating
287 experiment is broadly consistent with the postulated reversible equilibration of PD between
288 the gas-phase and the Teflon chamber walls.

289 Our SOA formation experiments are isothermal, but during the experiments the gas-phase
290 PD concentration (and thus activity) drops due to oxidation. To reproduce these conditions,
291 we used isothermal dilution to mimic the PD loss during SOA formation. We maintained
292 the chamber temperature at 22 °C and injected PD along with acetonitrile into the chamber,
293 and then measured their concentration ratio using the PTRMS. We used acetonitrile as a
294 passive tracer because it is highly volatile, should not have wall losses, and it is readily
295 measured with the PTRMS. After injecting PD and acetonitrile into the chamber, we turned
296 on a slow flow of dilution air, initially at a rate of 100 Lpm ($1\% \text{ min}^{-1}$) and later at a rate
297 of 300 Lpm ($3\% \text{ min}^{-1}$). These rates roughly bracket the loss rate of PD via OH oxidation
298 in our SOA formation experiments. We tracked the ratio of PD to acetonitrile. If the PD
299 sorbed to the Teflon chamber wall were released continuously because it was in (a
300 necessarily reversible) equilibrium, the PD concentration should fall more slowly than
301 acetonitrile, and the ratio of PD to acetonitrile should rise steadily. We show a simulation
302 of the expected signals in Fig. S1. As we show in Fig. 4, the concentrations of both PD and
303 acetonitrile steadily decreased after we started to flush the chamber. However, we did not
304 observe any increase in the PD to acetonitrile ratio; instead, the ratio remained almost
305 constant, and even showed a slight decrease. This suggests that PD does not return to the
306 gas phase from the Teflon walls at 22 °C, but instead still shows a modest loss to the



307 chamber walls. This indicates slow diffusion into the bulk Teflon, and is inconsistent with
308 the observations in Zhang et al. (Zhang et al., 2015).

309 During the dilution experiments, only after the PD concentration reached $2 \mu\text{g m}^{-3}$ (2% of
310 the initial concentration), 5.5h after we started dilution, did the ratio of PD to acetonitrile
311 start to increase. This confirms that PD can return to the gas phase from the chamber walls
312 even during isothermal dilution (or any other isothermal loss from the gas phase), but only
313 after substantial depletion of gas-phase concentrations of PD. Thus, while reversible
314 partitioning to the walls is the most straightforward explanation for the losses of PD we
315 have presented, and even the results of chamber heating are broadly consistent with this
316 explanation, we see no sign of reversibility under the conditions of our SOA formation
317 experiments. This is a paradox, for which we have no explanation.

318 Therefore, based on the empirical evidence we conclude that the measured decrease in PD
319 from PTRMS during SOA formation experiments is equal to the amount of PD oxidation,
320 and that no further correction for wall equilibration is necessary. There is no reason for the
321 PD to “know” whether its gas-phase concentration is decreasing because of reaction or
322 isothermal dilution, and so we conclude that the dilution experiment accurately simulates
323 the PD response to reactive loss. However, as a precaution against return flux after
324 substantial PD depletion, we shall limit our analysis to the first 1.5 e-folding lifetimes in
325 PD oxidation (we only use the data where the PD concentration is above 22% of its initial
326 value).

327 **3.2 Correction for particle wall loss.**



328 We conducted experiments to measure the SOA production from oxidation of PD by OH
329 radicals generated via HONO photolysis at five different initial PD concentrations: 1, 2,
330 4, 5, and 6 ppbv. We used equation 1 to calculate SOA mass yields (Y).

$$331 \quad Y = \frac{C_{SOA}}{\Delta C_{PD}} \quad (1)$$

332 where C_{SOA} is the measured mass concentration of SOA, and ΔC_{PD} is the mass
333 concentration of the reacted PD. We measured the PD concentration using PTRMS with a
334 unique mass fragment, $m/z=135$, and then calculated the ΔC_{PD} . As we have discussed, we
335 do not correct the measured concentration change in PD for any interaction with the
336 chamber walls. However, in order to calculate the C_{SOA} , we must also account for wall
337 losses of both particles and the condensable SOA products.

338 We employed three traditional methods to correct the particle wall loss, based on the
339 assumption that particles deposited to the chamber walls function as same as the suspended
340 particles for the SOA condensation. The corrected SOA production, C_{SOA} , is determined
341 by the ratio of suspended SOA (C_{SOA}^{sus}) to suspended ammonium sulfate seed (C_{seed}^{sus}) and
342 the initial concentration of ammonium-sulfate seed particles at time 0 h ($C_{seed}^{sus}(t = 0)$), as
343 shown in equation 2 (Hildebrandt et al., 2009).

$$344 \quad C_{SOA}(t) = \frac{C_{SOA}^{sus}(t)}{C_{seed}^{sus}(t)} C_{seed}^{sus}(t = 0) \quad (2)$$

345 The essential term is the SOA to seed ratio, $\frac{C_{SOA}^{sus}(t)}{C_{seed}^{sus}(t)}$. We calculated this ratio directly from
346 the organic and seed (sulfate + ammonium) concentrations measured by the HR-AMS
347 (method 1). We also used the SMPS data. We determined the $C_{seed}^{sus}(t)$ by applying an



348 exponential function to fit the measured decay of the pure ammonium-sulfate seeds before
349 photo-oxidation and then extrapolating that decay for the duration of each experiment
350 (method 2). We also calculated $C_{seed}^{sus}(t)$ by scaling the total particle number concentration
351 (method 3). Because both coagulation and nucleation were minimal during the
352 experiments, **we can correct for particle wall losses based on either mass or number**
353 **loss**. $C_{seed}^{sus}(t)$ is proportional to the total suspended particle number concentration. We
354 demonstrate method 2 and 3 in Fig. S2. We calculated $C_{SOA}^{sus}(t)$ as the difference between
355 the total particle mass and the $C_{seed}^{sus}(t)$ after correcting with the SOA density, 1.4 g cm^{-3} ,
356 which we calculated following the method of Nakao et al. (Nakao et al., 2013). As shown
357 in Fig. S3, the SOA to seed ratios from these three methods agree to within roughly 20%.
358 Consequently, we focused on the HR-AMS data (method 1) to perform the particle wall-
359 loss correction. We demonstrate one example of the temporal depletion of PD and SOA
360 formation in Fig. S4. Around 80% of PD reacted in the first hour. As mentioned previously,
361 we excluded all data where the PD concentration was less than 22% of its initial value from
362 the analysis; those data are plotted in gray.

363 **3.3 Correction for vapor wall loss.**

364 In addition to correcting for the loss of SOA as suspended particles, we also determine the
365 amount of condensable SOA vapors that condense directly to the Teflon chamber walls
366 after PD oxidation. This also reduces the observed SOA mass (Ye et al., 2016a; Krechmer
367 et al., 2016). If the condensing species are functionally non-volatile (their saturation ratios
368 are much larger than their particle-phase activity (Donahue et al., 2011b)), then
369 condensation to the suspended particles will be quasi-irreversible. Furthermore, for the
370 relatively low saturation concentration values required, there should be efficient wall losses



371 of the vapors. We thus assume that vapor wall losses are the same per unit condensation
372 sink as condensation to the suspended particles.

373 The condensation sink (CS) represents the loss frequency of vapors to the suspended
374 aerosol surface (Donahue et al., 2014); it can be thought of as the mean speed of the vapors
375 multiplied by the aerosol surface area, but modified for the gas-phase diffusion near the
376 particle surface and accounting for accommodation from the gas phase to the condensed
377 phase when that is rate limiting. We calculated the CS^P using equation 3 (Trump et al.,
378 2014),

$$387 \quad CS^P = \sum_k N_k \frac{\nu}{4} \pi d_{p,k}^2 \beta_k \quad (3)$$

379 where k refers to a particle size bin, N_k is the number concentration of particles in this
380 bin, ν is the mean thermal speed of the gas phase molecules, $d_{p,k}$ is the particle diameter,
381 and β_k is the transition-regime correction factor (Seinfeld and Pandis, 2006), which is a
382 function of the mass accommodation coefficient (α) and the mean free path of the organic
383 vapor in air. We used two accommodation coefficient values, 0.1 and 1, as limiting cases
384 as the available evidence suggests that $0.1 < \alpha < 1$ (Saleh et al., 2013). When $\alpha = 1$, the
385 condensation sink will be the same as the collision frequency between the gas molecules
386 and suspended particles.

388 Fig. 5 shows the suspended collision frequency versus time together with the number and
389 mass concentration of the suspended particles during an SOA formation experiment. The
390 collision frequency decreased initially due to particle wall losses. However, when the SOA
391 formation started, the SOA condensation increased the particle surface area and thus
392 increased the collision frequency. Later in the experiment, after the SOA formation was



393 almost complete, the particle wall loss again dominated and the collision frequency
394 decreased.

395 As shown in Scheme 1, the fraction of the oxidation products that initially condenses on
396 the suspended particles versus the chamber walls is determined by the ratio of the
397 suspended-particle condensation sink to the wall loss frequency (the wall condensation
398 sink). We previously measured a wall condensation sink for SVOCs in the CMU chamber
399 of 0.063 min^{-1} (Ye et al., 2016a). In Fig. 6 we compare the suspended-particle condensation
400 sink to the wall condensation sink for the two limiting values of the mass accommodation
401 coefficient: 0.1 and 1. When $\alpha = 1$, the suspended-particle condensation sink is much larger
402 than the wall condensation sink. In this case, only a very small fraction of the condensable
403 vapors are lost to the walls, at least initially. When $\alpha = 0.1$, the condensation sink of the
404 suspended particles and the chamber wall are comparable, which makes vapor wall loss
405 significant.

406 The interactions of semi-volatile oxidation products with the two different sinks
407 (suspended particles and the walls) can be complex, but products that are effectively
408 nonvolatile (with very high steady-state saturation ratios while the PD is being oxidized
409 (Donahue et al., 2011b)) should simply condense in proportion to the two condensation
410 sinks. In this case the mass that condenses on the walls is given by the mass observed to
411 condense on the suspended particles multiplied by the ratio of the wall condensation sink
412 to the suspended condensation sink. In Fig. 7 we show the products lost to the chamber
413 walls together with the SOA mass on the suspended particles and the particles lost to the
414 chamber walls. The direct deposition of the product vapors to the chamber wall may have



415 been as much as 1/3 of the total SOA mass at the lower limit of $\alpha = 0.1$ or as little as a few
416 percent if $\alpha = 1$. This vapor wall loss correction is thus significant but not excessively large.

417 **3.4 Correction for Delayed Condensation.**

418 Some condensable products will be accumulated in the gas phase in a steady state between
419 production and loss even if they have a very low saturation concentration. This is especially
420 significant early in an experiment when the oxidation rate (and thus production rate of
421 condensable vapors) is high (Donahue et al., 2011b). We can estimate this simply by
422 assuming that the condensable vapors are produced with a constant mass yield during PD
423 oxidation (that the mechanism is invariant) and that their saturation concentrations are very
424 low. We then apply a constant mass fraction to the amount of oxidized PD to estimate the
425 total concentration of condensable products in any phase. In Fig. 8, we show an example
426 calculation for $\alpha = 0.1$ and a constant mass yield of 0.88 as a dashed black curve; except
427 for early in the reaction, this provides a good match to the total condensed organics, but for
428 times less than 2 condensation lifetimes (21 min, indicated with the vertical dashed red line)
429 the observed SOA concentration is substantially less than 0.88 times the oxidized PD
430 (shown with the gray fill). The SOA mass yields during the first 10-20 minutes thus may
431 be underestimated if delayed condensation is ignored (Donahue et al., 2011b). On the other
432 hand, lower mass yields at lower OA concentrations can be interpreted in terms of semi-
433 volatile partitioning (Odum et al., 1996b; Donahue et al., 2005).

434 **3.5 Overall SOA mass yields from PD oxidation by OH radicals.**

435 In Fig. 9 we show calculated SOA mass yields from the 6 ppb PD experiment for three
436 cases, first considering only particle wall loss, and then treating both particle and vapor



437 wall loss for $\alpha = 1$ and for $\alpha = 0.1$. When $\alpha = 1$, the difference with and without vapor wall
438 losses (i.e. the first two cases) is very small. However, the mass yield increases by 30%
439 after correcting for vapor wall loss with $\alpha = 0.1$. We further estimate the delayed
440 condensation of ELVOC and LVOC products by finding the mass yield after two
441 condensation lifetimes, as illustrated in Fig. 8. The dashed horizontal lines indicate these
442 values. The true equilibrium SOA mass yields may be closer to the dashed lines than the
443 observed values due to delayed condensation.

444 In Fig. 10 we summarize data from five experiments with five different initial PD
445 concentrations: 1, 2, 4, 5, and 6 ppbv. The shaded area shows the range of SOA yields
446 when α values vary from 0.1 to 1. The instantaneous SOA mass yields are from 0.1 to 0.9
447 under the different SOA concentrations. As with the single case we present in Fig 9,
448 accounting for delayed condensation introduces a low-concentration asymptotic mass yield
449 between 0.4 and 0.8. The bottom line is that regardless of the mass accommodation
450 coefficient the SOA mass yields are high, with yields above 0.5 for $C_{\text{OA}} > 10 \mu\text{g m}^{-3}$. PD
451 oxidation by OH is thus a very efficient source of second-generation SOA.

452 The yields for $\alpha = 0.1$ accounting for delayed condensation are implausibly high, implying
453 that essentially all of the oxidation products have extremely low volatility and thus the only
454 reason for the observed rising mass yields is the dynamical delay early in the experiment
455 (which lasts for a relatively long time, ~20 min, due to the low condensation sink associated
456 with the low mass accommodation coefficient). On the other hand, the yields for $\alpha = 1$ are
457 plausible, implying that approximately half of the condensable oxidation products consist
458 of highly oxidized products formed via “auto oxidation” (Ehn et al., 2014) while the other
459 half are SVOCs that partition reversibly into the particles (Ye et al., 2016b; Ye et al., 2016c).



460 PD oxidation has much higher SOA mass yields than α -pinene oxidation. When $C_{OA} = 20$
461 $\mu\text{g m}^{-3}$, the SOA mass yields from α -pinene oxidation (by ozone or OH) are in the range
462 0.1–0.2 (Hallquist et al., 2009), whereas the SOA mass yields from PD oxidation by OH
463 are in the range 0.6–0.9, roughly five times larger. This finding holds regardless of wall
464 effects or other complications to quantitative interpretation of the product volatility
465 distribution, as those issues should be shared in common for each system. PD is a much
466 more effective source of SOA than α -pinene. This can be well explained by the structure
467 of PD. PD has two OH groups replacing the C=C double bond in α -pinene and yet it retains
468 the bicyclic backbone of that monoterpene. PD can be considered as a first-generation of
469 oxidation product of α -pinene; the likely atmospheric formation mechanism is hydrolysis
470 of a β -hydroxy nitrate formed after OH addition to the double bond in high- NO_x conditions.
471 When PD is oxidized, C-C bond cleavage is unlikely because of the bicyclic backbone.
472 Therefore, most PD oxidation products will be less volatile than PD and so more
473 condensable compared to comparable products from α -pinene. One exception to this is that
474 a major oxidation product of PD is oxy-pinocamphone, which is formed when OH abstracts
475 a hydrogen atom from the hydroxymethylene moiety in PD and O_2 immediately abstracts
476 the second hydrogen from the OH group, analogous to acetone formation from 2-propanol.
477 All of the other oxidation products of PD are plausibly condensable. It is thus sensible that
478 the molar yields of condensable products from PD oxidation are in the range 0.5–0.8 and
479 that the corresponding mass yields are significantly higher due to the added oxygen.

480 **3.6 Elemental analysis of the SOA.**

481 In Fig. 11, we plot the observed average carbon oxidation state, $\overline{OS}_{\text{C}} = 2O:C - H:C$, of
482 the SOA formed from PD as a function of the SOA mass concentration. \overline{OS}_{C} decreases as



483 the SOA mass increases, consistent with other studies of biogenic SOA (Donahue et al.,
484 2006; Shilling et al., 2009). The SOA that condenses very early in the experiment (at low
485 CO_A) is also highly oxidized. These promptly condensing organic products are ELVOCs or
486 LVOCs, with sufficiently low volatility to build up a high saturation ratio early in the
487 experiment. We also consistently observe a slight increase of \overline{OS}_C at the end of each
488 experiment. This may be due to the further oxidation (aging) of the products. The SOA
489 formed from a lower initial PD concentration also shows a higher \overline{OS}_C at the same SOA
490 concentration than the SOA formed from a higher initial PD charge. When the initial PD
491 concentration is low, the oxidation products may have more chance to react with OH
492 radicals and become more oxidized. However, it is also possible that the higher absolute
493 oxidation rate with higher PD concentrations drives up the gas-phase activity of SVOCs
494 with relatively lower \overline{OS}_C . Finally, it is possible that relatively more volatile (and less
495 oxidized) products are lost from SOA particles near the end of each experiment due to
496 sorption to the Teflon walls. As shown in Fig. S5, the ratio of organic to sulfate mass
497 decreased slightly after 2 hours, consistent with some SOA mass loss from the particles.

498 The composition findings are thus consistent with the mass-yield results for a relatively
499 high mass accommodation coefficient; there is a substantial mass yield of ELVOC and
500 LVOC products with very high \overline{OS}_C but also a significant yield of SVOC products,
501 probably with $\overline{OS}_\text{C} \lesssim 1$, that dilute the (E)LVOC condensate once conditions favor their
502 condensation.

503 In Fig. 11 we also compare the \overline{OS}_C of the SOA formed from PD in these experiments with
504 the \overline{OS}_C of PD oxidation products observed to participate in nucleation in the CLOUD



505 experiment. We plot values for CLOUD for molecular clusters with a single C_{10} molecule
506 and clusters with 4 C_{10} molecules; these values are based on molecular formulas in
507 negatively-charged clusters measured with an atmospheric pressure interface time of flight
508 mass spectrometer (APITOF) where the negative charge resides on a bisulfate anion
509 clustering with the (presumably neutral) C_{10} organic molecules formed from PD oxidation
510 (Schobesberger et al., 2013). The CLOUD values are thus based on a much different
511 technique than the highly fragmenting bulk particle electron ionization used in the AMS.
512 Despite these differences, the \overline{OS}_C values we observe are similar to those seen in the
513 CLOUD experiments. The oxidized organics observed in the CLOUD experiments have
514 molecular compositions $C_{10}H_xO_y$, where $x = 12, 14, 16$ and $y = 2–12$ (Schobesberger et al.,
515 2013). They appear in four progressive bands from growing clusters, which contained 1-4
516 C_{10} organic molecules, respectively. The \overline{OS}_C in the first band is relatively high, -0.2, but
517 this decreases to -0.8 for the fourth band. The decrease of OS_C with increasing cluster size
518 is consistent with what we observed in this study. We observed the \overline{OS}_C of the bulk SOA
519 at relatively high loading was around -0.7, which corresponds to the value measured in the
520 CLOUD experiments for larger clusters.

521 A self-consistent interpretation of these observations is that the least-volatile, early
522 condensing species forming SOA at low CoA in our experiments are ELVOCs that also
523 help form the smallest clusters in the CLOUD experiments, while the later condensing
524 species are LVOCs and SVOCs that also contribute to cluster growth in the CLOUD
525 experiment after initial nucleation.

526 **3.7 Representation of PD SOA in the two-dimensional volatility-oxidation space.**



527 Following the procedures in the literature (Presto and Donahue, 2006; Donahue et al.,
528 2011a), we mapped the distribution of volatility and \overline{OS}_C in the two-dimensional volatility-
529 oxidation space (2D-VBS). The constraints are relatively crude – just the observed mass
530 concentrations and bulk composition, and so we present 2D-VBS yield distribution that is
531 consistent with those constraints but still coarse grained. Specifically, we assume a long
532 "tail" toward extremely low volatility with roughly constant mass yield, a cluster of
533 products with slightly lower volatility than PD, and a large yield of oxy pinocamphone,
534 while is more volatile than PD. We present the full yield distribution, which conserves
535 carbon, in the supplemental material.

536 In Fig. 12 we show the product distribution, classifying organics in the broad classes of
537 ELVOCs, LVOCs, SVOCs or IVOCs. The top panel is a 2D representation. We show PD
538 as a filled yellow circle. The blue contours show the oxidation products from PD, with
539 higher values indicating higher yields. The lower panel is a consolidation of the two-
540 dimensional product contours into a 1D-VBS, showing the total mass yields in each
541 decadally spaced volatility bin. A majority of the condensed products fall to the upper left
542 of PD, with a lower volatility and higher \overline{OS}_C than PD. These compounds are produced
543 mostly by the addition of oxygen containing moieties to the PD backbone. However, some
544 products located on the right of PD show slightly higher \overline{OS}_C , but also higher volatility.
545 They may be formed by two possible reaction pathways. One is fragmentation, which
546 breaks the carbon backbone and produces smaller molecules with higher volatility than the
547 reactants. Another pathway is formation of oxy pinocamphone, as discussed above.

548 The products at the end of the low-volatility tail extending toward the upper left in the top
549 panel of Fig. 12 may contribute to the new-particle formation observed in the CLOUD



550 experiments. These ELVOCs, with $\log C^o < -3.5$ are the most likely to form new particles
551 because with constant mass yields the saturation ratio in each progressively less volatile
552 bin will grow by an order of magnitude. The \overline{OS}_C of these LVOC products ranges from 0
553 to 1, and they represent around 15 % of total SOA mass. This is consistent with CLOUD
554 observations showing that ~10% of the PD oxidation products could drive new-particle
555 formation (Schobesberger et al., 2013; Riccobono et al., 2014).

556 Employing the method of Chuang and Donahue (2016a), we conducted a dynamical
557 simulation of SOA production following oxidation of 6 ppb PD in the CMU chamber,
558 assuming a mass accommodation coefficient $\alpha = 1$. As shown in Fig. 13, the simulation
559 describes the formation of condensable vapors and subsequent production of SOA mass.
560 The suspended SOA mass in the simulation matches the smog-chamber data very well. The
561 particle mass and SOA vapors lost to the Teflon chamber wall are also comparable with
562 the calculated values from the experimental data. Especially during the first 15 minutes,
563 the simulation shows there is a large fraction of condensable SOA vapors in the gas phase.
564 This agrees with the observed condensation delay due to the condensation sink timescale.

565 **4 Conclusions**

566 Our studies show that oxidation of pinanediol, a semi-volatile surrogate for first-generation
567 oxidation products of monoterpenes, can produce SOA with very high mass yields. The
568 SOA is also highly oxidized. This is thus a model system to describe chemical aging of
569 first-generation SOA. Along with previously studied model systems for first-generation
570 products, this shows that aging of semi-volatile SOA is a significant source of additional
571 SOA mass, with higher mass yields typical of less volatile first-generation products. The
572 second-generation oxidation products with sufficiently low volatility represent 15% of the



573 total SOA mass in a 2D-VBS model that reproduces the chamber data; these may contribute
574 to new-particle formation. The oxidation state of the chamber SOA produced from
575 oxidation of PD is also consistent with the observations during new-particle formation
576 experiments at CERN. Thus, while first-generation oxidation is a substantial source of both
577 SOA mass and new-particle formation, ongoing oxidation of first-generation vapors, which
578 typically comprise the large majority of the first-generation oxidation products from
579 common precursors, should also be considered as a significant source of both particle
580 number and mass.

581 *Competing interests.* The authors declare that they have no conflict of interest.

582 *Acknowledgments.* This research was supported by grant AGS1136479 and AGS1447056,
583 from the National Science Foundation. The High-Resolution Aerosol Mass Spectrometer
584 was purchased with Major Research Instrumentation funds from NSF CBET0922643 and
585 the Wallace Research Foundation.

586 **References**

- 587 Chacon-Madrid, H. J., Presto, A. A., and Donahue, N. M.: Functionalization vs. fragmentation: n-
588 aldehyde oxidation mechanisms and secondary organic aerosol formation, *Physical Chemistry*
589 *Chemical Physics*, 12, 13975-13982, 10.1039/C0CP00200C, 2010.
- 590 Chacon-Madrid, H. J., and Donahue, N. M.: Fragmentation vs. functionalization: chemical aging
591 and organic aerosol formation, *Atmospheric Chemistry and Physics*, 11, 10553-10563,
592 10.5194/acp-11-10553-2011, 2011.
- 593 Chacon-Madrid, H. J., Murphy, B. N., Pandis, S. N., and Donahue, N. M.: Simulations of smog-
594 chamber experiments using the two-dimensional volatility basis set: linear oxygenated
595 precursors, *Environmental Science & Technology*, 46, 11179-11186, 10.1021/es3017232, 2012.
- 596 Chacon-Madrid, H. J., Henry, K. M., and Donahue, N. M.: Photo-oxidation of pinonaldehyde at
597 low NO_x: from chemistry to organic aerosol formation, *Atmospheric Chemistry and Physics*, 13,
598 3227-3236, 10.5194/acp-13-3227-2013, 2013.
- 599 Chuang, W. K., and Donahue, N. M.: Dynamic Consideration of Smog Chamber Experiments,
600 *Atmospheric Chemistry and Physics*, 17, 10019-10036, 10.5194/acp-17-10019-2017, 2017.
- 601 Chuang, W. K., and Donahue, N. M.: A two-dimensional volatility basis set – Part 3: Prognostic
602 modeling and NO_x dependence, *Atmospheric Chemistry and Physics*, 16, 123-134, 10.5194/acp-
603 16-123-2016, 2016b.
- 604 Cubison, M. J., Ortega, A. M., Hayes, P. L., Farmer, D. K., Day, D., Lechner, M. J., Brune, W. H.,
605 Apel, E., Diskin, G. S., Fisher, J. A., Fuelberg, H. E., Hecobian, A., Knapp, D. J., Mikoviny, T.,
606 Riemer, D., Sachse, G. W., Sessions, W., Weber, R. J., Weinheimer, A. J., Wisthaler, A., and
607 Jimenez, J. L.: Effects of aging on organic aerosol from open biomass burning smoke in aircraft
608 and laboratory studies, *Atmospheric Chemistry and Physics*, 11, 12049-12064, 10.5194/acp-11-
609 12049-2011, 2011.
- 610 Donahue, N., Robinson, A., Trump, E., Riipinen, I., and Kroll, J.: Volatility and Aging of
611 Atmospheric Organic Aerosol, in: *Atmospheric and Aerosol Chemistry*, edited by: McNeill, V.
612 F., and Ariya, P. A., *Topics in Current Chemistry*, Springer Berlin Heidelberg, 97-143, 2014.
- 613 Donahue, N. M., Huff Hartz, K. E., Chuong, B., Presto, A. A., Stanier, C. O., Rosenhorn, T.,
614 Robinson, A. L., and Pandis, S. N.: Critical factors determining the variation in SOA yields from
615 terpene ozonolysis: A combined experimental and computational study, *Faraday Discussions*,
616 130, 295-309, 10.1039/B417369D, 2005.
- 617 Donahue, N. M., Robinson, A. L., Stanier, C. O., and Pandis, S. N.: Coupled Partitioning, Dilution,
618 and Chemical Aging of Semivolatile Organics, *Environmental Science & Technology*, 40, 2635-
619 2643, 10.1021/es052297c, 2006.
- 620 Donahue, N. M., Epstein, S. A., Pandis, S. N., and Robinson, A. L.: A two-dimensional volatility
621 basis set: 1. organic-aerosol mixing thermodynamics, *Atmospheric Chemistry and Physics*, 11,
622 3303-3318, 10.5194/acp-11-3303-2011, 2011a.
- 623 Donahue, N. M., Trump, E. R., Pierce, J. R., and Riipinen, I.: Theoretical constraints on pure vapor-
624 pressure driven condensation of organics to ultrafine particles, *Geophysical Research Letters*,
625 38, L16801, 10.1029/2011GL048115, 2011b.
- 626 Donahue, N. M., Trump, E. R., Pierce, J. R., and Riipinen, I.: Theoretical constraints on pure vapor-
627 pressure driven condensation of organics to ultrafine particles, *Geophysical Research Letters*,
628 38, L16801, 10.1029/2011GL048115, 2011c.
- 629 Donahue, N. M., Henry, K. M., Mentel, T. F., Kiendler-Scharr, A., Spindler, C., Bohn, B., Brauers,
630 T., Dorn, H. P., Fuchs, H., Tillmann, R., Wahner, A., Saathoff, H., Naumann, K.-H., Möhler,
631 O., Leisner, T., Müller, L., Reinnig, M.-C., Hoffmann, T., Salo, K., Hallquist, M., Frosch, M.,
632 Bilde, M., Tritscher, T., Barmet, P., Praplan, A. P., DeCarlo, P. F., Dommen, J., Prévôt, A. S.
633 H., and Baltensperger, U.: Aging of biogenic secondary organic aerosol via gas-phase OH
634 radical reactions, *Proceedings of the National Academy of Sciences*, 109, 13503-13508,
635 10.1073/pnas.1115186109, 2012a.



- 636 Donahue, N. M., Kroll, J. H., Pandis, S. N., and Robinson, A. L.: A two-dimensional volatility
 637 basis set – Part 2: Diagnostics of organic-aerosol evolution, *Atmospheric Chemistry and Physics*,
 638 12, 615–634, 10.5194/acp-12-615-2012, 2012b.
 639 Donahue, N. M., Chuang, W., Epstein, S. A., Kroll, J. H., Worsnop, D. R., Robinson, A. L., Adams,
 640 P. J., and Pandis, S. N.: Why do organic aerosols exist? Understanding aerosol lifetimes using
 641 the two-dimensional volatility basis set, *Environmental Chemistry*, 10, 151–157, 2013.
 642 Duplissy, J., Merikanto, J., Franchin, A., Tsagkogeorgas, G., Kangasluoma, J., Wimmer, D.,
 643 Vuollekoski, H., Schobesberger, S., Lehtipalo, K., Flagan, R. C., Brus, D., Donahue, N. M.,
 644 Vehkamäki, H., Almeida, J., Amorim, A., Barmet, P., Bianchi, F., Breitenlechner, M., Dunne,
 645 E. M., Guida, R., Henschel, H., Junninen, H., Kirkby, J., Kurten, A., Kupc, A., Määttänen, A.,
 646 Makhmutov, V., Mathot, S., Nieminen, T., Onnela, A., Praplan, A. P., Riccobono, F., Rondo,
 647 L., Steiner, G., Tome, A., Walther, H., Baltensperger, U., Carslaw, K. S., Dommen, J., Hansel,
 648 A., Petäjä, T., Sipilä, M., Stratmann, F., Vrtala, A., Wagner, P. E., Worsnop, D. R., Curtius, J.,
 649 and Kulmala, M.: Effect of ions on sulfuric acid-water binary particle formation: 2.
 650 Experimental data and comparison with QC-normalized classical nucleation theory, *Journal of
 651 Geophysical Research: Atmospheres*, 121, 1752–1775, 10.1002/2015JD023539, 2016.
 652 Ehn, M., Thornton, J. A., Kleist, E., Sipila, M., Junninen, H., Pullinen, I., Springer, M., Rubach, F.,
 653 Tillmann, R., Lee, B., Lopez-Hilfiker, F., Andres, S., Acir, I.-H., Rissanen, M., Jokinen, T.,
 654 Schobesberger, S., Kangasluoma, J., Kontkanen, J., Nieminen, T., Kurten, T., Nielsen, L. B.,
 655 Jorgensen, S., Kjaergaard, H. G., Canagaratna, M., Maso, M. D., Berndt, T., Petaja, T., Wahner,
 656 A., Kerminen, V.-M., Kulmala, M., Worsnop, D. R., Wildt, J., and Mentel, T. F.: A large source
 657 of low-volatility secondary organic aerosol, *Nature*, 506, 476–479, 10.1038/nature13032, 2014.
 658 Hallquist, M., Wenger, J. C., Baltensperger, U., Rudich, Y., Simpson, D., Claeys, M., Dommen, J.,
 659 Donahue, N. M., George, C., Goldstein, A. H., Hamilton, J. F., Herrmann, H., Hoffmann, T.,
 660 Iinuma, Y., Jang, M., Jenkin, M. E., Jimenez, J. L., Kiendler-Scharr, A., Maenhaut, W.,
 661 McFiggans, G., Mentel, T. F., Monod, A., Prévôt, A. S. H., Seinfeld, J. H., Surratt, J. D.,
 662 Szmigielski, R., and Wildt, J.: The formation, properties and impact of secondary organic
 663 aerosol: current and emerging issues, *Atmospheric Chemistry and Physics*, 9, 5155–5236,
 664 10.5194/acp-9-5155-2009, 2009.
 665 Henry, K. M., and Donahue, N. M.: Photochemical aging of α -pinene secondary organic aerosol:
 666 Effects of OH radical sources and photolysis, *The Journal of Physical Chemistry A*, 116, 5932–
 667 5940, 10.1021/jp210288s, 2012.
 668 Hildebrandt, L., Donahue, N. M., and Pandis, S. N.: High formation of secondary organic aerosol
 669 from the photo-oxidation of toluene, *Atmospheric Chemistry and Physics*, 9, 2973–2986, 2009.
 670 Jang, M., and Kamens, R. M.: Newly characterized products and composition of secondary aerosols
 671 from the reaction of α -pinene with ozone, *Atmospheric Environment*, 33, 459–474, 1999.
 672 Jaoui, M., and Kamens, R. M.: Mass balance of gaseous and particulate products analysis from α -
 673 pinene/NO x /air in the presence of natural sunlight, *Journal of Geophysical Research: Atmospheres*, 106, 12541–12558, 10.1029/2001JD900005, 2001.
 674 Kanakidou, M., Seinfeld, J. H., Pandis, S. N., Barnes, I., Dentener, F. J., Facchini, M. C., Dingdenen,
 675 R. V., Ervens, B., Nenes, A., Nielsen, C. J., Swietlicki, E., Putaud, J. P., Balkanski, Y., Fuzzi,
 676 S., Horth, J., Moortgat, G. K., Winterhalter, R., Myhre, C. E. L., Tsigaridis, K., Vignati, E.,
 677 Stephanou, E. G., and Wilson, J.: Organic aerosol and global climate modelling: a review,
 678 *Atmospheric Chemistry and Physics*, 5, 1053–1123, 2005.
 679 Kirkby, J., Curtius, J., Almeida, J., Dunne, E., Duplissy, J., Ehrhart, S., Franchin, A., Gagne, S.,
 680 Ickes, L., Kurten, A., Kupc, A., Metzger, A., Riccobono, F., Rondo, L., Schobesberger, S.,
 681 Tsagkogeorgas, G., Wimmer, D., Amorim, A., Bianchi, F., Breitenlechner, M., David, A.,
 682 Dommen, J., Downard, A., Ehn, M., Flagan, R. C., Haider, S., Hansel, A., Hauser, D., Jud, W.,
 683 Junninen, H., Kreissl, F., Kvashin, A., Laaksonen, A., Lehtipalo, K., Lima, J., Lovejoy, E. R.,
 684 Makhmutov, V., Mathot, S., Mikkila, J., Minginette, P., Mogo, S., Nieminen, T., Onnela, A.,
 685 Pereira, P., Petaja, T., Schnitzhofer, R., Seinfeld, J. H., Sipila, M., Stozhkov, Y., Stratmann, F.,
 686



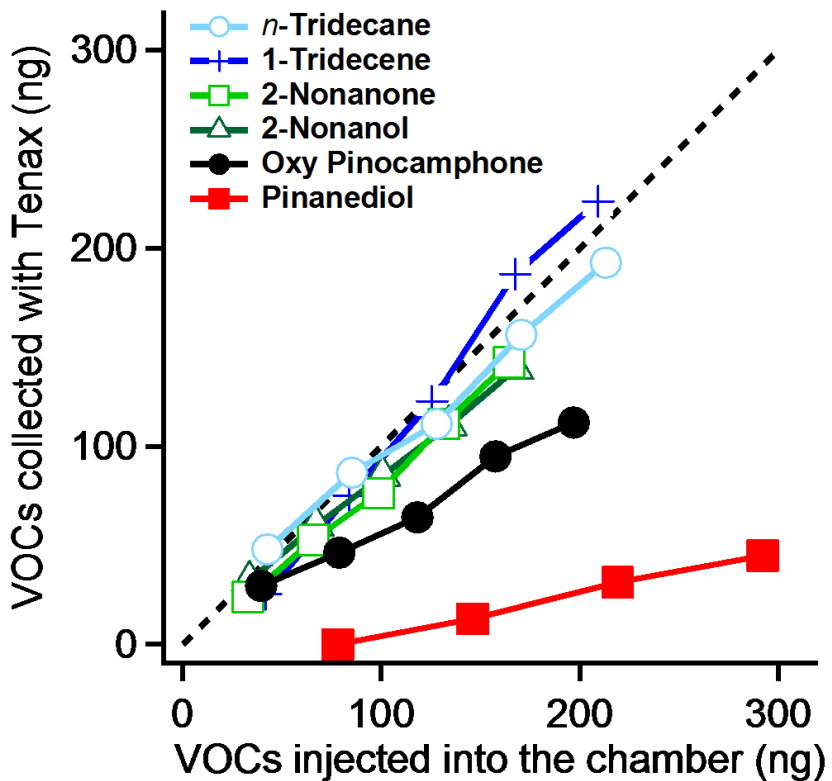
- 687 Tome, A., Vanhanen, J., Viisanen, Y., Vrtala, A., Wagner, P. E., Walther, H., Weingartner, E.,
688 Wex, H., Winkler, P. M., Carslaw, K. S., Worsnop, D. R., Baltensperger, U., and Kulmala, M.:
689 Role of sulphuric acid, ammonia and galactic cosmic rays in atmospheric aerosol nucleation,
690 *Nature*, 476, 429-433, 2011.
- 691 Krechmer, J. E., Pagonis, D., Ziemann, P. J., and Jimenez, J. L.: Quantification of Gas-Wall
692 Partitioning in Teflon Environmental Chambers Using Rapid Bursts of Low-Volatility Oxidized
693 Species Generated in Situ, *Environmental Science & Technology*, 50, 5757-5765,
694 10.1021/acs.est.6b00606, 2016.
- 695 Kroll, J. H., Smith, J. D., Che, D. L., Kessler, S. H., Worsnop, D. R., and Wilson, K. R.:
696 Measurement of fragmentation and functionalization pathways in the heterogeneous oxidation
697 of oxidized organic aerosol, *Physical Chemistry Chemical Physics*, 11, 8005-8014,
698 10.1039/B905289E, 2009.
- 699 Lambe, A. T., Ahern, A. T., Williams, L. R., Slowik, J. G., Wong, J. P. S., Abbatt, J. P. D., Brune,
700 W. H., Ng, N. L., Wright, J. P., Croasdale, D. R., Worsnop, D. R., Davidovits, P., and Onasch,
701 T. B.: Characterization of aerosol photooxidation flow reactors: heterogeneous oxidation,
702 secondary organic aerosol formation and cloud condensation nuclei activity measurements,
703 *Atmospheric Measurement Techniques*, 4, 445-461, 10.5194/amt-4-445-2011, 2011.
- 704 Matsunaga, A., and Ziemann ‡, P. J.: Gas-Wall Partitioning of Organic Compounds in a Teflon
705 Film Chamber and Potential Effects on Reaction Product and Aerosol Yield Measurements,
706 *Aerosol Science and Technology*, 44, 881-892, 10.1080/02786826.2010.501044, 2010.
- 707 May, A. A., Saleh, R., Hennigan, C. J., Donahue, N. M., and Robinson, A. L.: Volatility of Organic
708 Molecular Markers Used for Source Apportionment Analysis: Measurements and Implications
709 for Atmospheric Lifetime, *Environmental Science & Technology*, 46, 12435-12444,
710 10.1021/es302276t, 2012.
- 711 Müller, L., Reinnig, M. C., Naumann, K. H., Saathoff, H., Mentel, T. F., Donahue, N. M., and
712 Hoffmann, T.: Formation of 3-methyl-1,2,3-butanetricarboxylic acid via gas phase oxidation of
713 pinonic acid – a mass spectrometric study of SOA aging, *Atmospheric Chemistry and Physics*,
714 12, 1483-1496, 10.5194/acp-12-1483-2012, 2012.
- 715 Nakao, S., Tang, P., Tang, X., Clark, C. H., Qi, L., Seo, E., Asa-Awuku, A., and Cocker Iii, D.:
716 Density and elemental ratios of secondary organic aerosol: Application of a density prediction
717 method, *Atmospheric Environment*, 68, 273-277, 2013.
- 718 Odum, J. R., Hoffmann, T., Bowman, F., Collins, D., Flagan, R. C., and Seinfeld, J. H.: Gas/particle
719 partitioning and secondary organic aerosol yields, *Environmental Science & Technology*, 30,
720 2580-2585, 1996a.
- 721 Odum, J. R., Hoffmann, T., Bowman, F., Collins, D., Flagan, R. C., and Seinfeld, J. H.: Gas/Particle
722 Partitioning and Secondary Organic Aerosol Yields, *Environmental Science & Technology*, 30,
723 2580-2585, 10.1021/es950943+, 1996b.
- 724 Pandis, S. N., Paulson, S. E., Seinfeld, J. H., and Flagan, R. C.: Aerosol formation in the
725 photooxidation of isoprene and β-pinene, *Atmospheric Environment*, 25A, 997-1008, 1991.
- 726 Pope, C. A., Ezzati, M., and Dockery, D. W.: Fine-Particulate Air Pollution and Life Expectancy
727 in the United States, *New England Journal of Medicine*, 360, 376-386,
728 doi:10.1056/NEJMsa0805646, 2009.
- 729 Presto, A. A., and Donahue, N. M.: Investigation of α-Pinene + Ozone Secondary Organic Aerosol
730 Formation at Low Total Aerosol Mass, *Environmental Science & Technology*, 40, 3536-3543,
731 10.1021/es052203z, 2006.
- 732 Qi, L., Nakao, S., and Cocker, D. R.: Aging of secondary organic aerosol from α-pinene ozonolysis:
733 Roles of hydroxyl and nitrate radicals, *Journal of the Air & Waste Management Association*, 62,
734 1359-1369, 10.1080/10962247.2012.712082, 2012.
- 735 Riccobono, F., Schobesberger, S., Scott, C. E., Dommen, J., Ortega, I. K., Rondo, L., Almeida, J.,
736 Amorim, A., Bianchi, F., Breitenlechner, M., David, A., Downard, A., Dunne, E. M., Duplissy,
737 J., Ehrhart, S., Flagan, R. C., Franchin, A., Hansel, A., Junninen, H., Kajos, M., Keskinen, H.,



- 738 Kupc, A., Kürten, A., Kvashin, A. N., Laaksonen, A., Lehtipalo, K., Makhmutov, V., Mathot,
 739 S., Nieminen, T., Onnella, A., Petäjä, T., Praplan, A. P., Santos, F. D., Schallhart, S., Seinfeld, J.
 740 H., Sipilä, M., Spracklen, D. V., Stozhkov, Y., Stratmann, F., Tomé, A., Tsagkogeorgas, G.,
 741 Vaattovaara, P., Viisanen, Y., Vrtala, A., Wagner, P. E., Weingartner, E., Wex, H., Wimmer,
 742 D., Carslaw, K. S., Curtius, J., Donahue, N. M., Kirkby, J., Kulmala, M., Worsnop, D. R., and
 743 Baltensperger, U.: Oxidation Products of Biogenic Emissions Contribute to Nucleation of
 744 Atmospheric Particles, *Science*, 344, 717-721, 10.1126/science.1243527, 2014.
- 745 Robinson, E. S., Saleh, R., and Donahue, N. M.: Organic aerosol mixing observed by single-particle
 746 mass spectrometry, *The Journal of Physical Chemistry A*, 117, 13935-13945, 10.1021/jp405789t,
 747 2013.
- 748 Saleh, R., Donahue, N. M., and Robinson, A. L.: Time Scales for Gas-Particle Partitioning
 749 Equilibration of Secondary Organic Aerosol Formed from Alpha-Pinene Ozonolysis,
 750 *Environmental Science & Technology*, 47, 5588-5594, 10.1021/es400078d, 2013.
- 751 Schobesberger, S., Junninen, H., Bianchi, F., Lönn, G., Ehn, M., Lehtipalo, K., Dommen, J.,
 752 Ehrhart, S., Ortega, I. K., Franchin, A., Nieminen, T., Riccobono, F., Hutterli, M., Duplissy, J.,
 753 Almeida, J., Amorim, A., Breitenlechner, M., Downard, A. J., Dunne, E. M., Flagan, R. C.,
 754 Kajos, M., Keskinen, H., Kirkby, J., Kupc, A., Kürten, A., Kurtén, T., Laaksonen, A., Mathot,
 755 S., Onnella, A., Praplan, A. P., Rondo, L., Santos, F. D., Schallhart, S., Schnitzhofer, R., Sipilä,
 756 M., Tomé, A., Tsagkogeorgas, G., Vehkamäki, H., Wimmer, D., Baltensperger, U., Carslaw, K.,
 757 S., Curtius, J., Hansel, A., Petäjä, T., Kulmala, M., Donahue, N. M., and Worsnop, D. R.:
 758 Molecular understanding of atmospheric particle formation from sulfuric acid and large
 759 oxidized organic molecules, *Proceedings of the National Academy of Sciences*, 110, 17223-
 760 17228, 10.1073/pnas.1306973110, 2013.
- 761 Seinfeld, J. H., and Pandis, S. N.: *Atmospheric chemistry and physics — from air pollution to
 762 climate change*, 2nd ed., John Wiley & Sons, New York, 2006.
- 763 Shilling, J. E., Chen, Q., King, S. M., Rosenoern, T., Kroll, J. H., Worsnop, D. R., DeCarlo, P. F.,
 764 Aiken, A. C., Sueper, D., Jimenez, J. L., and Martin, S. T.: Loading-dependent elemental
 765 composition of α -pinene SOA particles, *Atmospheric Chemistry and Physics*, 9, 771-782,
 766 10.5194/acp-9-771-2009, 2009.
- 767 Solomon, S. Q., D.; Manning, M.; Alley, R. B.; Berntsen, T.; Bindoff, N. L.; Chen, Z.; Chidthaisong,
 768 A.; Gregory, J. M.; Hegerl, G. C.: Climate change 2007: The physical science basis, contribution
 769 of working group 1 to the fourth assessment report of the Intergovernmental Panel on Climate
 770 Change, 2007.
- 771 Tkacik, D. S., Lambe, A. T., Jathar, S., Li, X., Presto, A. A., Zhao, Y., Blake, D., Meinardi, S.,
 772 Jayne, J. T., Croteau, P. L., and Robinson, A. L.: Secondary Organic Aerosol Formation from
 773 in-Use Motor Vehicle Emissions Using a Potential Aerosol Mass Reactor, *Environmental
 774 Science & Technology*, 48, 11235-11242, 10.1021/es502239v, 2014.
- 775 Tröstl, J., Chuang, W. K., Gordon, H., Heinritzi, M., Yan, C., Molteni, U., Ahlm, L., Frege, C.,
 776 Bianchi, F., Wagner, R., Simon, M., Lehtipalo, K., Williamson, C., Craven, J. S., Duplissy, J.,
 777 Adamov, A., Almeida, J., Bernhammer, A.-K., Breitenlechner, M., Brilke, S., Dias, A., Ehrhart,
 778 S., Flagan, R. C., Franchin, A., Fuchs, C., Guida, R., Gysel, M., Hansel, A., Hoyle, C. R.,
 779 Jokinen, T., Junninen, H., Kangasluoma, J., Keskinen, H., Kim, J., Krapf, M., Kürten, A.,
 780 Laaksonen, A., Lawler, M., Leiminger, M., Mathot, S., Möhler, O., Nieminen, T., Onnella, A.,
 781 Petäjä, T., Piel, F. M., Miettinen, P., Rissanen, M. P., Rondo, L., Sarnela, N., Schobesberger, S.,
 782 Sengupta, K., Sipilä, M., Smith, J. N., Steiner, G., Tomé, A., Virtanen, A., Wagner, A. C.,
 783 Weingartner, E., Wimmer, D., Winkler, P. M., Ye, P., Carslaw, K. S., Curtius, J., Dommen, J.,
 784 Kirkby, J., Kulmala, M., Riipinen, I., Worsnop, D. R., Donahue, N. M., and Baltensperger, U.:
 785 The role of low-volatility organic compounds in initial particle growth in the atmosphere, *Nature*,
 786 533, 527-531, 10.1038/nature18271, 2016.

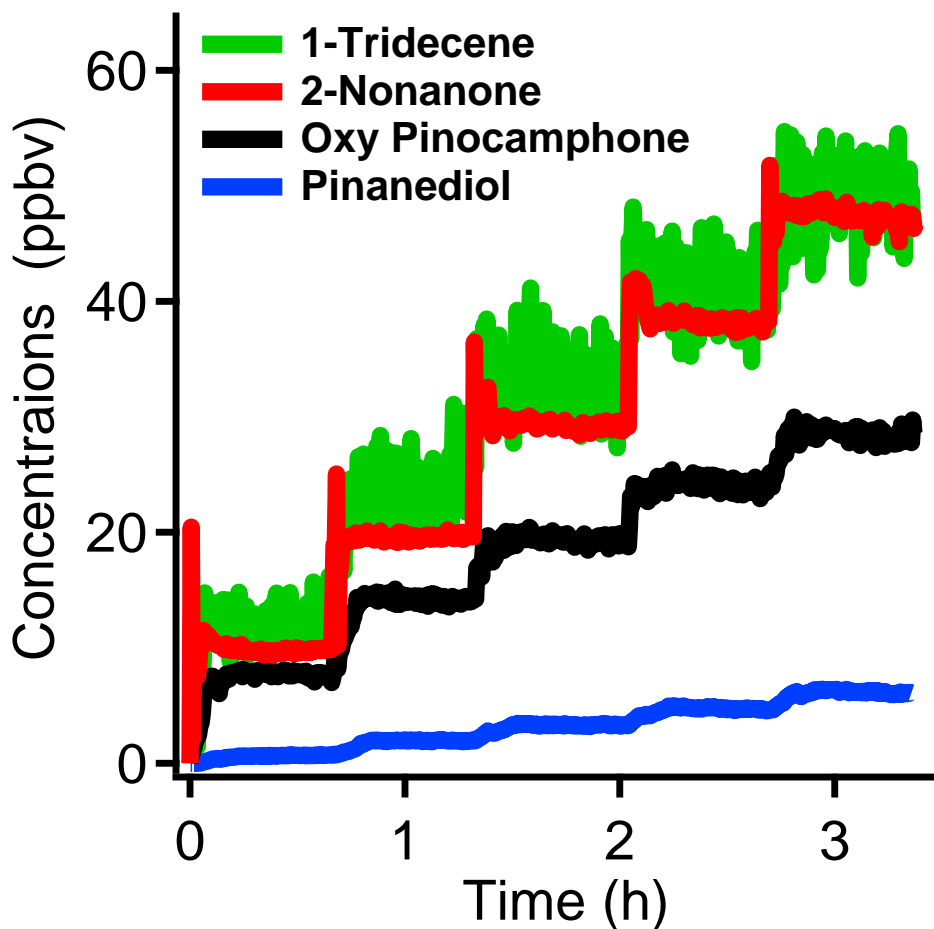


- 787 Trump, E. R., Riipinen, I., and Donahue, N. M.: Interactions between atmospheric ultrafine
788 particles and secondary organic aerosol mass: a model study, *Boreal Environment Research*, 19,
789 352–362, 2014.
- 790 Trump, E. R., Epstein, S. A., Riipinen, I., and Donahue, N. M.: Wall effects in smog chamber
791 experiments: A model study, *Aerosol Science and Technology*, 50, 1180-1200,
792 10.1080/02786826.2016.1232858, 2016.
- 793 Wong, J. P. S., Lee, A. K. Y., Slowik, J. G., Cziczo, D. J., Leaitch, W. R., Macdonald, A., and
794 Abbatt, J. P. D.: Oxidation of ambient biogenic secondary organic aerosol by hydroxyl radicals:
795 Effects on cloud condensation nuclei activity, *Geophysical Research Letters*, 38, L22805,
796 10.1029/2011GL049351, 2011.
- 797 Ye, P., Ding, X., Hakala, J., Hofbauer, V., Robinson, E. S., and Donahue, N. M.: Vapor wall loss
798 of semi-volatile organic compounds in a Teflon chamber, *Aerosol Science and Technology*, 50,
799 822-834, 10.1080/02786826.2016.1195905, 2016a.
- 800 Ye, P., Ding, X., Ye, Q., Robinson, E. S., and Donahue, N. M.: Uptake of Semivolatile Secondary
801 Organic Aerosol Formed from α -Pinene into Nonvolatile Polyethylene Glycol Probe Particles,
802 *The Journal of Physical Chemistry A*, 120, 1459-1467, 10.1021/acs.jpca.5b07435, 2016b.
- 803 Ye, Q., Robinson, E. S., Ding, X., Ye, P., Sullivan, R. C., and Donahue, N. M.: Mixing of secondary
804 organic aerosols versus relative humidity, *Proceedings of the National Academy of Sciences*,
805 113, 12649-12654, 10.1073/pnas.1604536113, 2016c.
- 806 Zhang, Q., Jimenez, J. L., Canagaratna, M. R., Allan, J. D., Coe, H., Ulbrich, I., Alfarra, M. R.,
807 Takami, A., Middlebrook, A. M., Sun, Y. L., Dzepina, K., Dunlea, E., Docherty, K., DeCarlo,
808 P. F., Salcedo, D., Onasch, T., Jayne, J. T., Miyoshi, T., Shimojo, A., Hatakeyama, S.,
809 Takegawa, N., Kondo, Y., Schneider, J., Drewnick, F., Borrmann, S., Weimer, S., Demerjian,
810 K., Williams, P., Bower, K., Bahreini, R., Cottrell, L., Griffin, R. J., Rautiainen, J., Sun, J. Y.,
811 Zhang, Y. M., and Worsnop, D. R.: Ubiquity and dominance of oxygenated species in organic
812 aerosols in anthropogenically-influenced Northern Hemisphere midlatitudes, *Geophysical
813 Research Letters*, 34, L13801, 10.1029/2007GL029979, 2007.
- 814 Zhang, X., McVay, R. C., Huang, D. D., Dalleska, N. F., Aumont, B., Flagan, R. C., and Seinfeld,
815 J. H.: Formation and evolution of molecular products in α -pinene secondary organic aerosol,
816 *Proceedings of the National Academy of Sciences*, 112, 14168-14173,
817 10.1073/pnas.1517742112, 2015.
- 818 Zhao, Y., Hennigan, C. J., May, A. A., Tkacik, D. S., de Gouw, J. A., Gilman, J. B., Kuster, W. C.,
819 Borbon, A., and Robinson, A. L.: Intermediate-Volatility Organic Compounds: A Large Source
820 of Secondary Organic Aerosol, *Environmental Science & Technology*, 48, 13743-13750,
821 10.1021/es5035188, 2014.



822

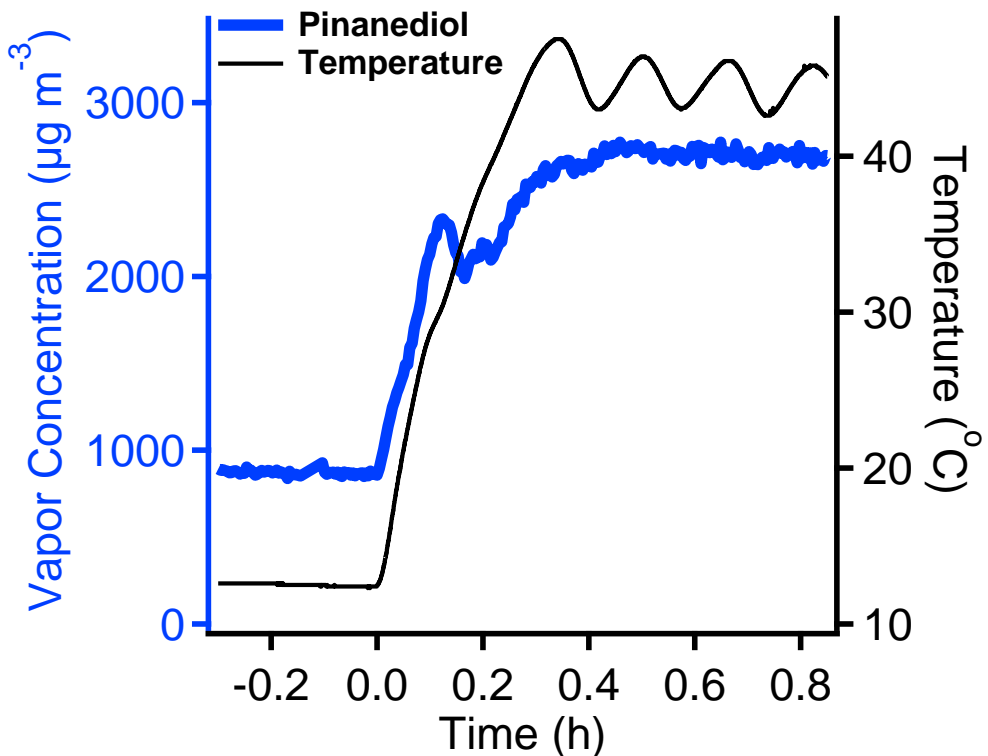
823 **Figure 1.** The gas phase concentrations of *n*-tridecane, 1-tridecene, 2-nonenone,
824 2-Nonanol, oxy pinocamphone and pinanediol in the chamber measured by TDGC/MS. Compared to the amount of organics
825 injected into the chamber, *n*-tridecane, 1-tridecene and 2-nonenone and 2-Nonanol show almost no vapor wall
826 loss. Oxy pinocamphone and pinanediol show 43% and 86% loss, respectively.



827

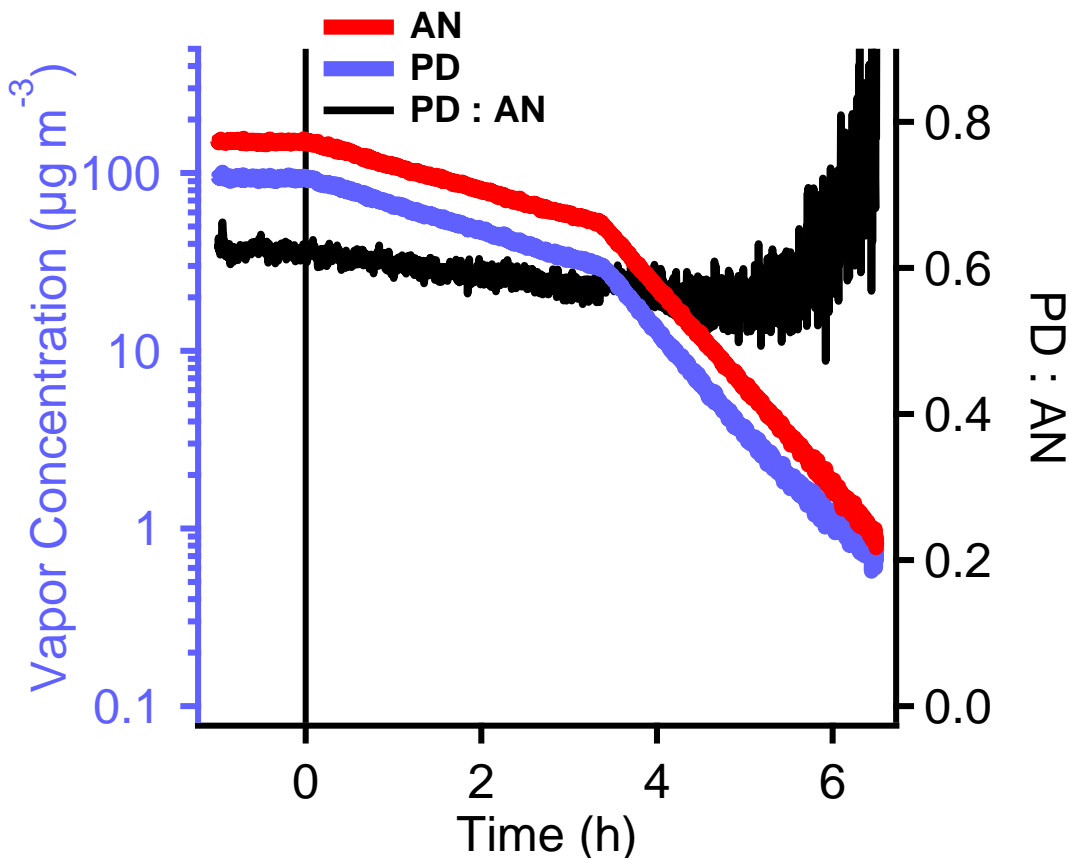
828

829 **Figure 2.** The temporal concentrations of the organics after we injected a series of aliquots of 1-tridencene,
830 2-nonenone, oxy pinocamphone and pinanediol into the chamber in increments of 11 ppbv (at 100% injection
831 efficiency). Each injection resulted in a similar increase of all organics. The similar increase indicates that
832 oxy pinocamphone and pinanediol may have constant wall loss factors in the concentration range studied in
this work.



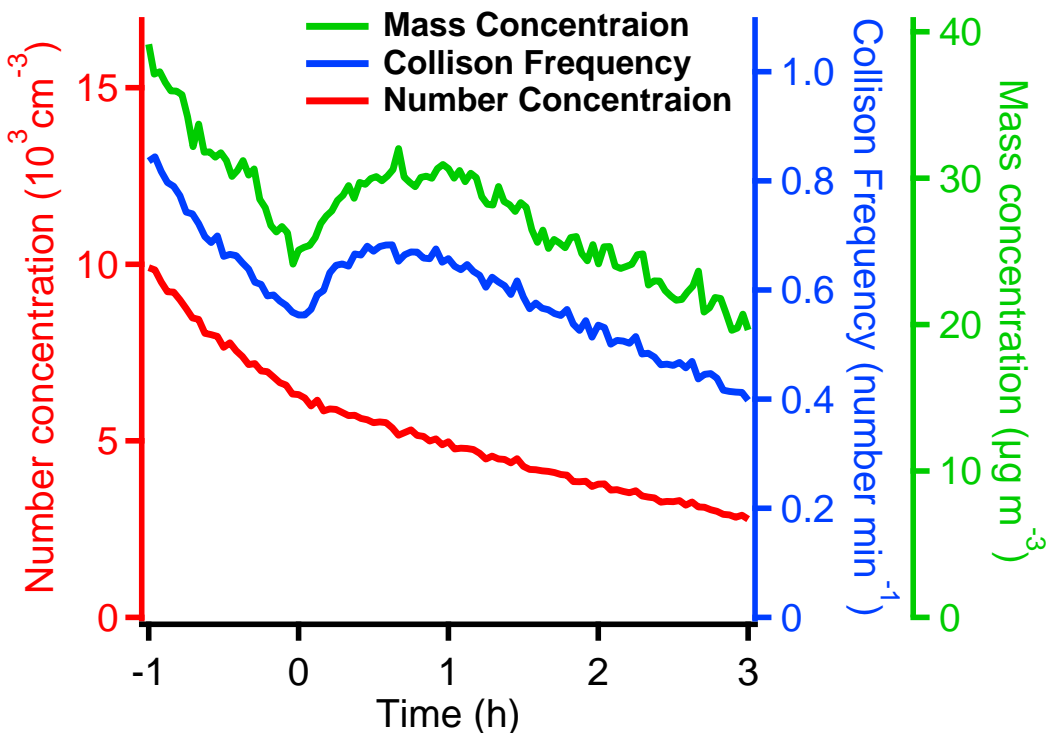
833

834 **Figure 3.** The increase of the pinanediol vapor concentration after increasing the chamber temperature from
835 13 $^{\circ}\text{C}$ to 44 $^{\circ}\text{C}$. The concentration of PD increased 2.5-3 times and reached a constant value after temperature
836 stabilized at 44 $^{\circ}\text{C}$. The increase of the PD concentration shows that PD can come out from the chamber walls
837 at higher temperature.



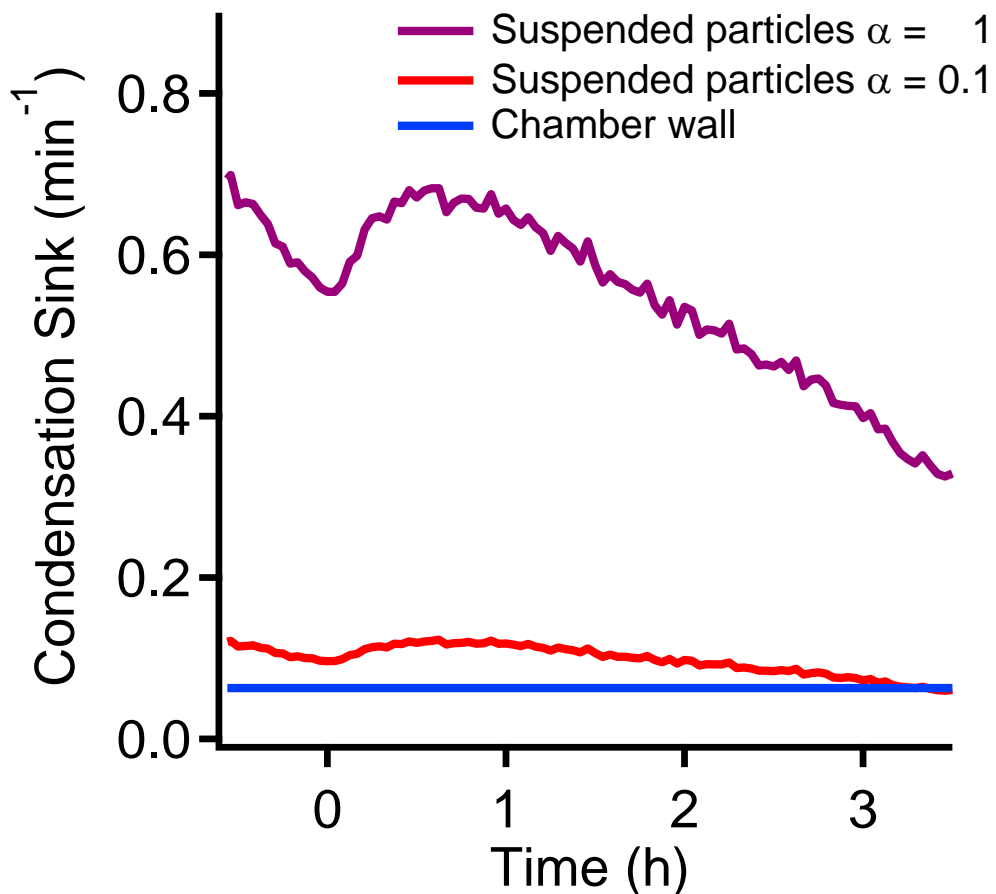
838

839 **Figure 4.** The change of PD and AN concentrations during isothermal dilution of the chamber with fresh air,
840 which mimics the depletion of PD during the SOA formation. The ratio of PD to AN shows very small change
841 until the PD concentration dropped below $2 \mu\text{g m}^{-3}$. This indicates that PD does not return to the gas phase
842 from the Teflon at 22°C , but instead still shows a modest loss to the chamber walls. So no further correction
843 for the release or loss of PD is necessary when studying the SOA formation.



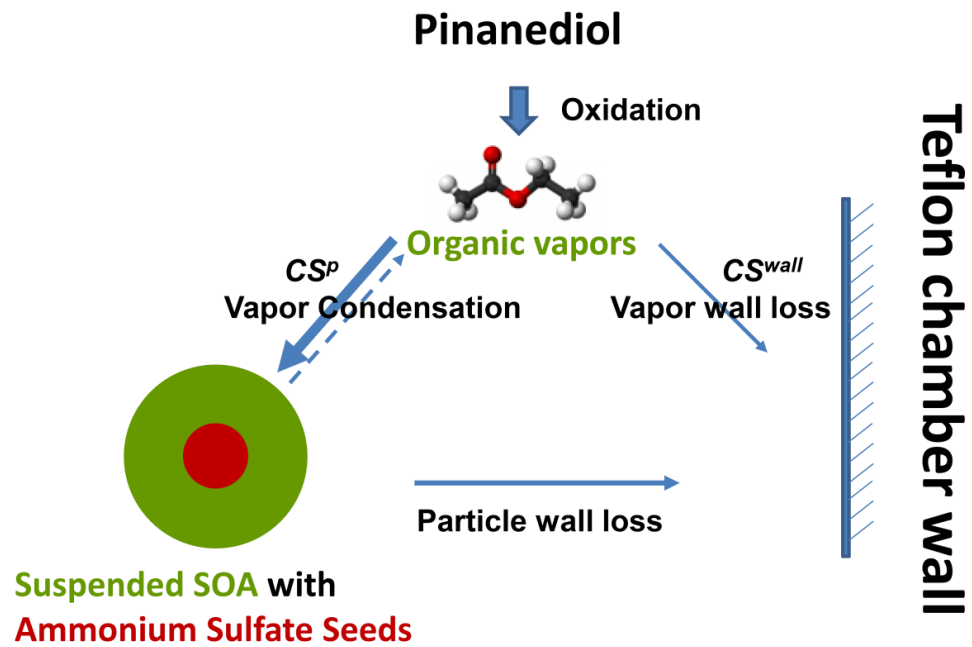
844

845 **Figure 5.** The change of collision frequency and number, mass concentration of the suspended particles
846 during the SOA formation. The collision frequency has the same value as condensation sink when $\alpha=1$. After
847 the SOA formation started at 0h, the SOA mass condensed on the particles increased the particle surface
848 areas and increased the collision frequency. We also observed the increase of the total mass concentrations.
849 The particle number concentration always followed the exponential decay which indicated the nucleation
850 may be minimal.



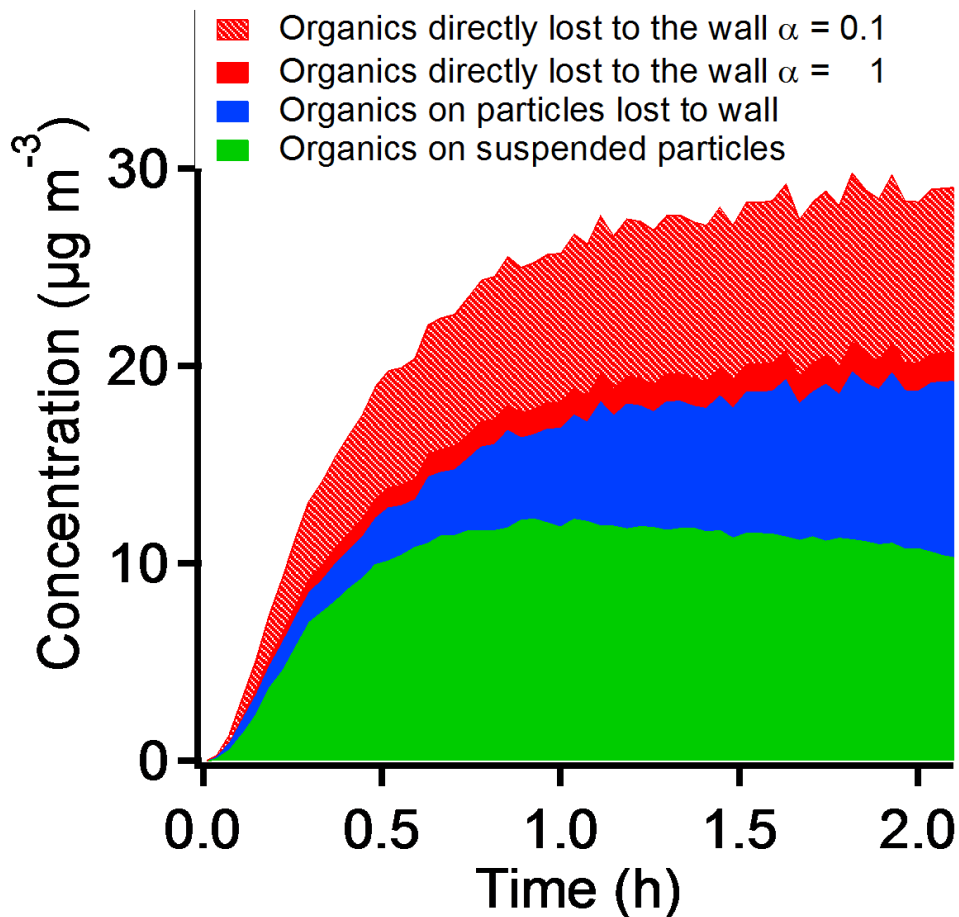
851

852 **Figure 6.** The difference of the condensation sink between the chamber wall with the suspended particles
853 when the mass accommodation coefficient is 0.1 or 1. When $\alpha = 1$, the condensaiton sink of the suspended
854 particles is much larger than the wall condensation sink. When $\alpha = 0.1$, the two values are on a similar level
855 which indicates that the vapor wall loss may be very significant.



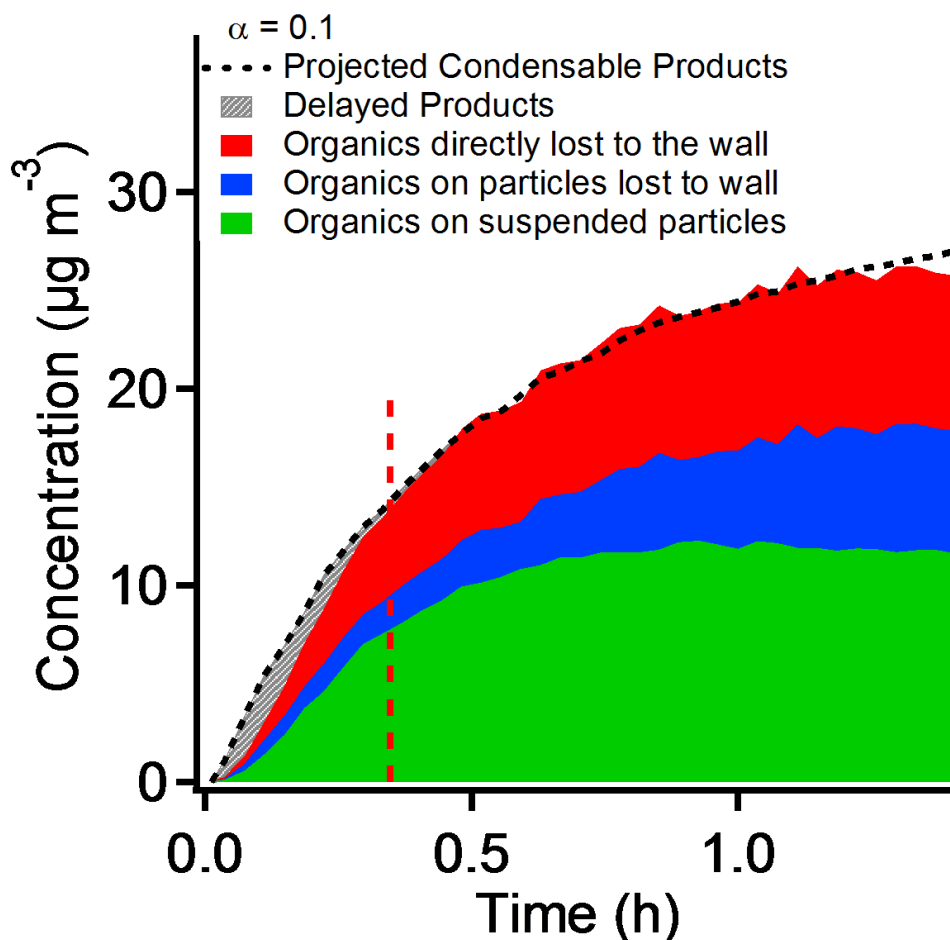
856

857 **Scheme 1.** The competition of vapor deposition on the suspended particles and the Teflon chamber walls.
858 The fraction of the oxidation products deposited on the suspended particles and the chamber wall are
859 determined by the condensation sink to the particles and the chamber walls



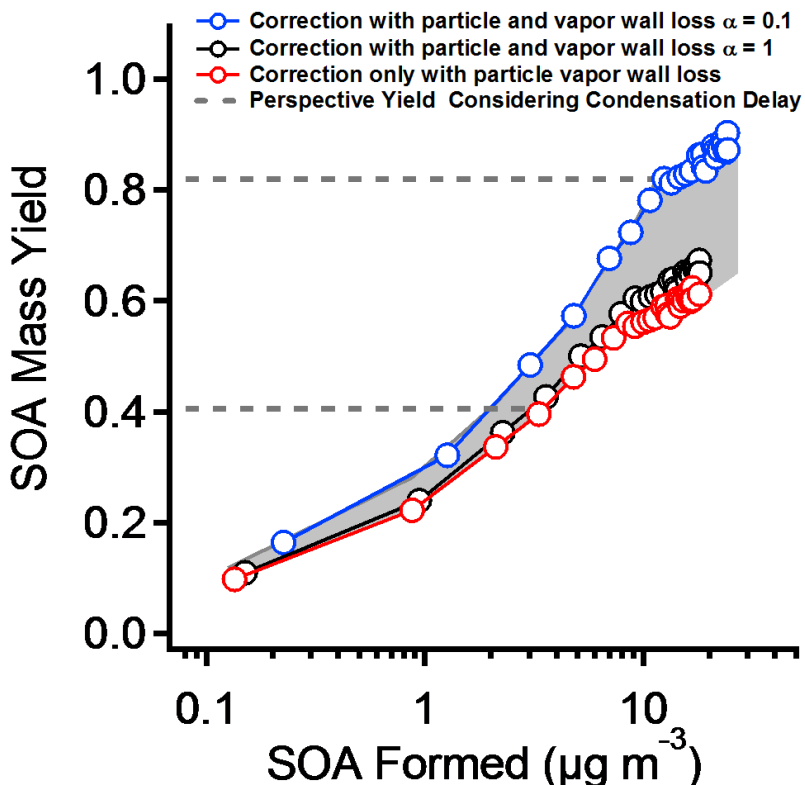
860

861 **Figure 7.** The SOA mass on the suspended particles, lost to chamber wall due to particle wall loss and
862 direct vapor deposition on the chamber wall. When $\alpha = 0.1$, the SOA mass lost to the chamber wall through
863 the direct vapor deposition may have one third of the total SOA mass. When $\alpha = 1$, the vapor wall loss may
864 not be significant.



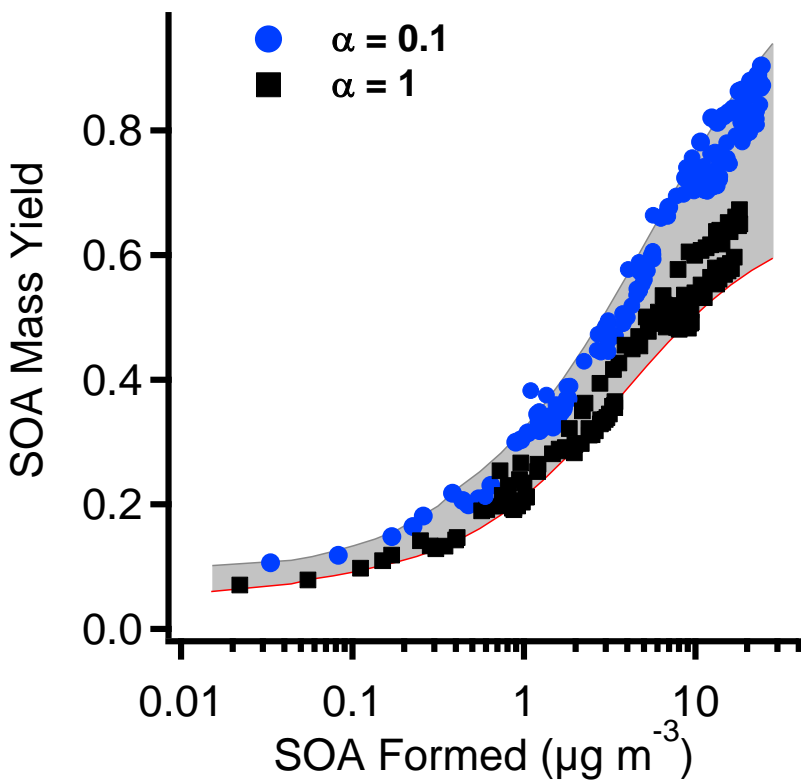
865
866
867
868
869
870

Figure 8. The discrepancy of the observed SOA caused by the condensation delay. The black dash line shows the estimated concentration of condensable vapors from the reacted PD. The dashed area at 0-0.3 hours shows the difference between formed vapors and the observed SOA. This gap may be caused by the diffusion time of vapor molecules to reach the surface of the particles or the chamber walls. This delay may result in a lower measured SOA mass yield at the early stage of the experiment.



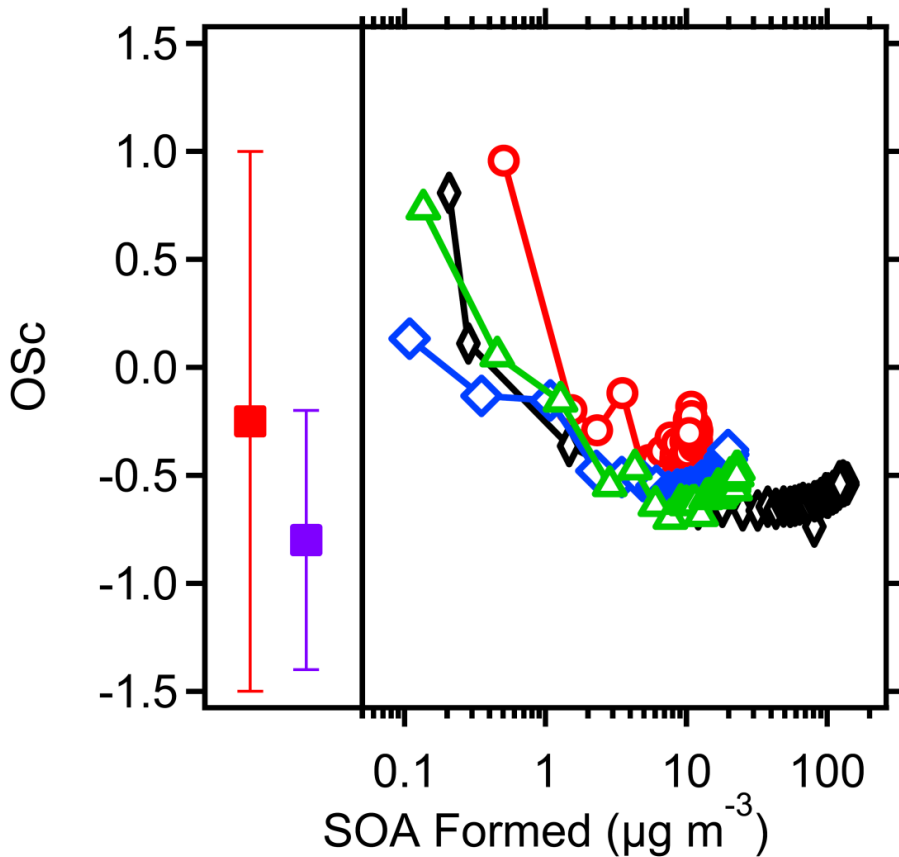
871

872 **Figure 9.** The SOA yield from pinanediol photo-oxidation after correction for particle wall loss and vapor
 873 wall loss using three different methods: correction for particle wall-loss only; correction for vapor wall loss
 874 with $\alpha = 1$; and correction for vapor wall loss with $\alpha = 0.1$. For the first two methods the mass yields are
 875 similar. For the third, when $\alpha = 0.1$, the mass yield is 30% higher than for the other two methods. The
 876 horizontal dashed lines indicate the mass yields at a time equal to twice the gas-phase lifetime of vapors
 877 due to condensation or wall loss. Before this time (below the lines) the measured SOA yields may be biased
 878 low due to the delay between production and condensation to the suspended particles.



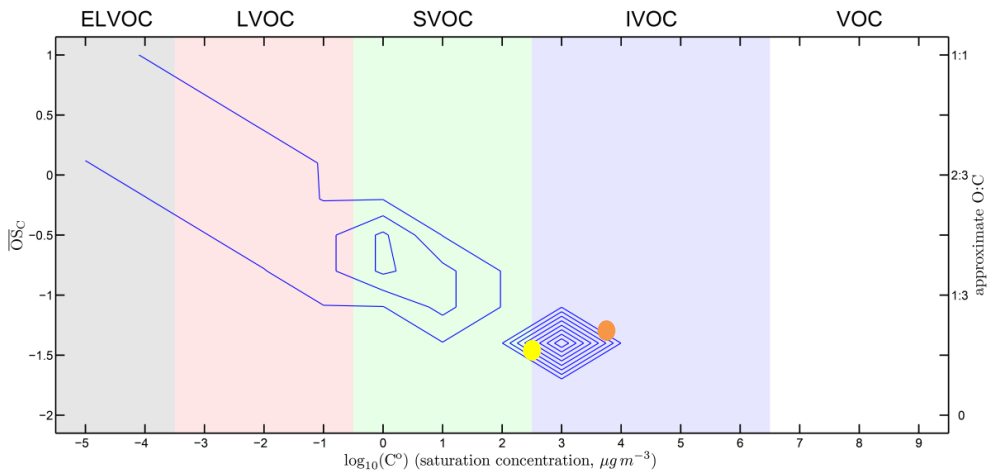
879

880 **Figure 10.** The summary of all the SOA mass yield after correcting both particle and vapor wall loss.
881 The initial PD concentrations are 1,2,4,5, and 6 ppbv. The shade area shows the yield range when
882 α varies from 0.1 to 1.

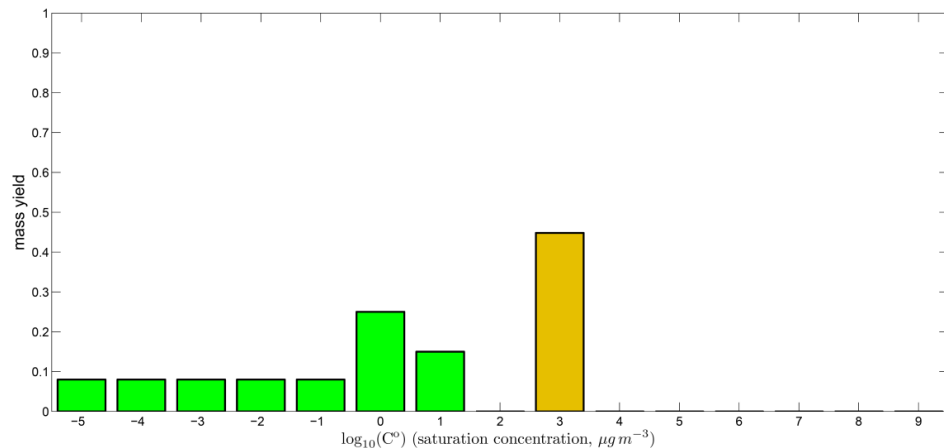


883

884 **Figure 11.** The $\overline{\text{OS}}_{\text{C}}$ of the SOA from PD with initial concentrations at 4, 5, 6 and 12 ppb on the right panel.
885 The left panel shows the $\overline{\text{OS}}_{\text{C}}$ of the oxidation products from PD in the clusters observed in the CLOUD
886 experiments, which contained 1 (red solid square) and 4 (blue solid square) C_{10} organics. The SOA formed
887 at the very early stage (low yields) shows highly oxidized. The $\overline{\text{OS}}_{\text{C}}$ in this study are comparable to the results
888 from the CLOUD experiments.



889



890

891

Figure 12. Representation of the oxidation products from PD in the two-dimensional volatility-oxidation space for a mass accommodation coefficient $\alpha = 1$. We group organics in the broad classes of ELVOCs, LVOCs, SVOCs or IVOCs. The top panel is a 2D representation. PD is shown as a yellow dot. The blue contours show the oxidation products from PD, with higher values indicating higher yields. The lower panel is a 1D consolidation of the 2D product contours, showing the total mass yields in each volatility bin. The major products spread toward the upper left from PD, with increased oxidation state and decreased volatility. The products near to the upper left corner, in the ELVOC region, may contribute to new-particle formation observed in the CLOUD experiments. They constitute around 15% of the total SOA mass. Some products may undergo fragmentation or functional group change, such as converting an alcohol group to a carbonyl group, as with oxy pinocamphone, which is shown in orange.

892

893

894

895

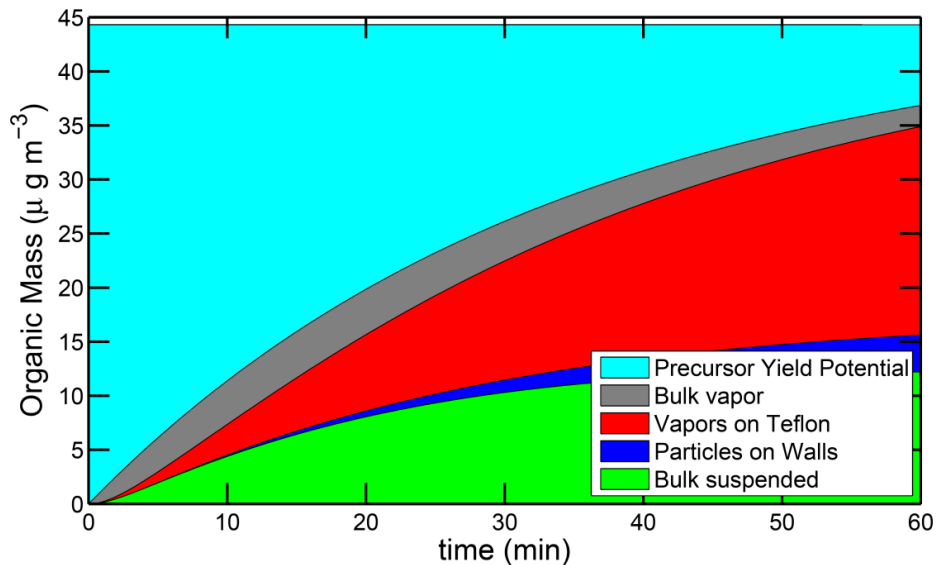
896

897

898

899

900



901
902
903
904
905

Figure 13. Dynamical simulation of the SOA production from 6 ppb of PD with a mass accommodation coefficient $\alpha=1$. The simulation treats five different reservoirs: unreacted precursor, vapors, suspended particles, deposited particles, and sorption to teflon, as shown in the legend. The simulation reproduces the SOA observed on the suspended particles.